

# On the Role of the Bridging Dicyanamidobenzene Ligand in a New Binuclear Ruthenium Complex: $[\{\text{Ru}(\text{tpy})(\text{thd})\}_2(\mu\text{-dicyd})][\text{PF}_6]$ with $\text{tpy} = 2,2':6',2''\text{-Terpyridine}$ and $\text{thd} = 2,2,6,6\text{-Tetramethyl-3,5-heptanedione}$

Muriel Fabre,<sup>†</sup> Joël Jaud,<sup>†</sup> Mohamed Hliwa,<sup>†,‡</sup> Jean-Pierre Launay,<sup>†</sup> and Jacques Bonvoisin<sup>\*,†</sup>

CEMES/CNRS, NanoSciences Group, BP 94347, 29 rue Jeanne Marvig, 31055 Toulouse Cedex 4, France, and Faculté des Sciences, Université Hassan II-Mohammédia, BP 7955-Sidi Othman, Casablanca, Morocco

Received June 16, 2006

The dicyanamidobenzene-bridge diruthenium complex  $[\{\text{Ru}(\text{tpy})(\text{thd})\}_2(\mu\text{-dicyd})][\text{PF}_6]$  ( $[\mathbf{3}][\text{PF}_6]$ ) (dicyd = 1,4-dicyanamidobenzene, tpy = 2,2':6',2''-terpyridine, thd = 2,2,6,6-tetramethyl-3,5-heptanedione) and its mononuclear counterpart  $[\text{Ru}(\text{tpy})(\text{thd})(\text{lpcyd})]$  ( $\mathbf{2}$ ) [ $\text{lpcyd} = 4\text{-iodophenylcyanamide anion} (\text{lpcyd}^-)$ ] were synthesized and fully characterized. Cyclic voltammetry of  $\mathbf{3}$  showed the presence of four reversible one-electron redox couples. UV–vis–NIR spectroelectrochemistry and EPR spectroscopy of the electrogenerated paramagnetic intermediates were used to ascertain the oxidation-state distribution. The stable starting dinuclear complex  $\mathbf{3}^+$  is found to be a ligand-centered anion radical as shown by EPR spectroscopy, magnetic susceptibility measurements, and DFT calculations. Oxidation of  $\mathbf{3}^+$  to  $\mathbf{3}^{2+}$  led to an EPR silent system due to substantial intramolecular antiferromagnetic interaction of the electron spins carried by the low spin ruthenium(III) atom and the bridging anion radical dicyanido ( $\text{dicyd}^{\cdot-}$ ), an observation which was supported by UV–vis–NIR, X-ray structure, and DFT calculations. Complex  $\mathbf{3}^{3+}$  presented an EPR spectra consistent with a total effective spin  $S = 1/2$  issued from an antiferromagnetic interaction of electron spins carried by two low spin ruthenium(III) atoms and the bridging anion radical  $\text{dicyd}^{\cdot-}$  in accordance with UV–vis–NIR. This study shows that the dicyanamidobenzene bridging ligand has indubitably a noninnocent behavior.

## 1. Introduction

The development of newer classes of dinuclear metal complexes incorporating suitable bridging ligands which lead to the formation of stable mixed valence (MV) states has attracted considerable research in recent years.<sup>1,2</sup> This was primarily due to the relevance for biological processes,<sup>3</sup> molecular electronics,<sup>4</sup> and theoretical studies of electron-transfer kinetics.<sup>5</sup> The bridging ligand (BL) mediated inter-

metallic electronic communication takes place through their  $\pi$ -symmetry orbitals either by electron-transfer (ET) or hole-transfer (HT) mechanisms.<sup>6</sup>

Dicyanamidobenzene ligands are prone to be well-suited for intramolecular electro- and magnetocommunications<sup>7–10</sup> via an HT mechanism.<sup>7,10–13</sup> To achieve a strong electronic interaction it is necessary to match the energy of the metal-

\* To whom correspondence should be addressed. E-mail: jbonvoisin@cemes.fr. Phone: +33 5 62 25 78 52. Fax: +33 5 62 25 79 99.

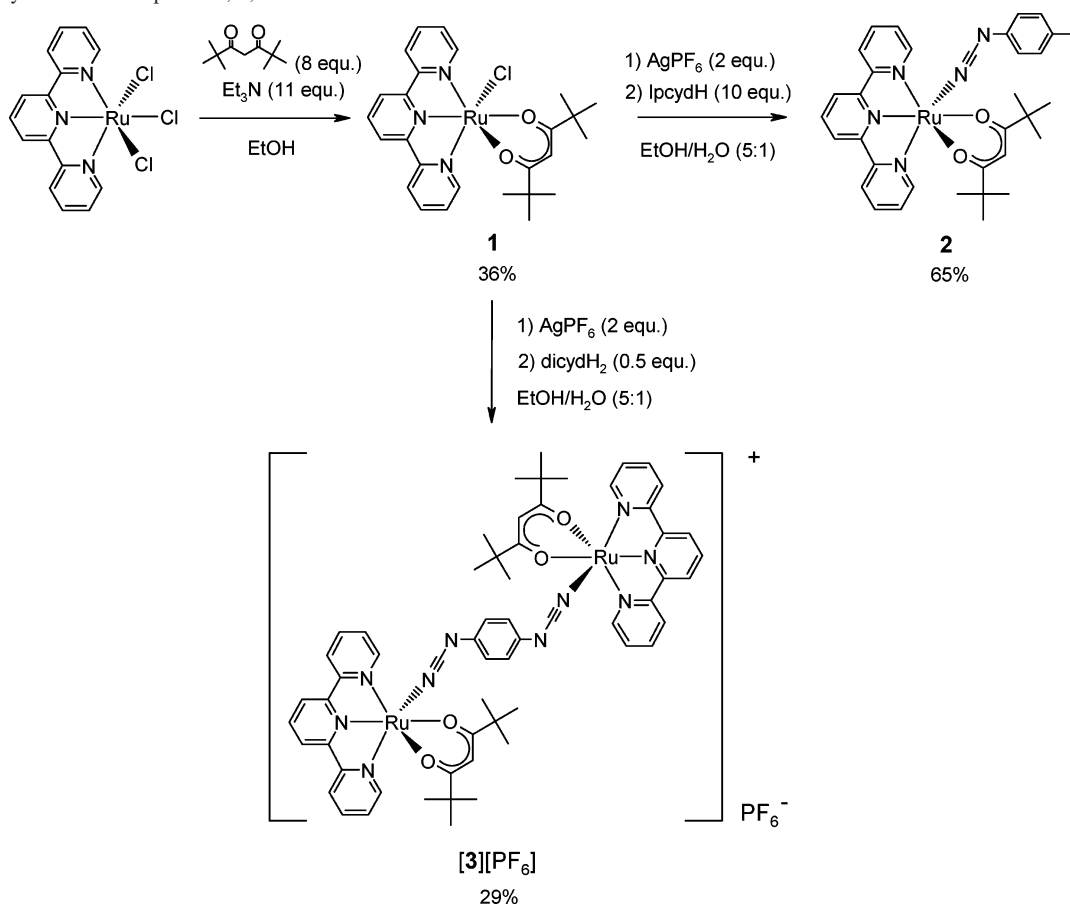
<sup>†</sup> CEMES/CNRS, NanoSciences Group.

<sup>‡</sup> Université Hassan II-Mohammédia.

- (1) McCleverty, J. A.; Ward, M. D. *Acc. Chem. Res.* **1998**, *31* (12), 842.
- (2) Kaim, W.; Klein, A.; Gloeckle, M. *Acc. Chem. Res.* **2000**, *33* (11), 755.
- (3) Solomon, E. I.; Brunold, T. C.; Davis, M. I.; Kemsley, J. N.; Lee, S. K.; Lehnert, N.; Neese, F.; Skulan, A. J.; Yang, Y. S.; Zhou, J. *Chem. Rev.* **2000**, *100*, 235.
- (4) Launay, J.-P. *Chem. Soc. Rev.* **2001**, *30*, 386. Launay, J.-P.; Coudret, C. Wires Based on Metal Complexes. In *Electron Transfer in Chemistry*; Balzani, V., Ed.; Wiley-VCH: Weinheim, 2001; Vol. 5, pp 3. Ward, M. D. *Chem. Soc. Rev.* **1995**, *24* (2), 121. Paul, F.; Lapinte, C. *Coord. Chem. Rev.* **1998**, *178–180*, 431. Low, P. J. *Dalton Trans.* **2005**, 2821.

- (5) Brunschwig, B. S.; Sutin, N. *Coord. Chem. Rev.* **1999**, *187*, 233.
- (6) Kaim, W.; Kasack, V. *Inorg. Chem.* **1990**, *29* (23), 4696.
- (7) Aquino, M. A. S.; Lee, F. L.; Gabe, E. J.; Bensimon, C.; Greedan, J. E.; Crutchley, R. J. *J. Am. Chem. Soc.* **1992**, *114*, (13), 5130.
- (8) Crutchley, R. J. *Adv. Inorg. Chem.* **1994**, *41*, 273. Crutchley, R. J. *Compr. Coord. Chem. II* **2004**, *2*, 785.
- (9) Rezvani, A. R.; Evans, C. E. B.; Crutchley, R. J. *Inorg. Chem.* **1995**, *34* (18), 4600.
- (10) Evans, C. E. B.; Yap, G. P. A.; Crutchley, R. J. *Inorg. Chem.* **1998**, *37* (24), 6161.
- (11) Evans, C. E. B.; Naklicki, M. L.; Rezvani, A. R.; White, C. A.; Kondratiev, V. V.; Crutchley, R. J. *J. Am. Chem. Soc.* **1998**, *120* (50), 13096.
- (12) Naklicki, M. L.; Crutchley, R. J. *Inorg. Chim. Acta* **1994**, *225* (1–2), 123.
- (13) Rezvani, A. R.; Bensimon, C.; Crompton, B.; Reber, C.; Greedan, J. E.; Kondratiev, V. V.; Crutchley, R. J. *Inorg. Chem.* **1997**, *36* (15), 3322.

Scheme 1. Synthesis of Complexes 1, 2, and 3



based redox orbital with an appropriate BL orbital, such that delocalization in the MV state can be optimized by a superexchange process involving the BL: here, HT through the BL HOMO (highest occupied molecular orbital). A fundamental question is whether such a ligand is innocent or not during this process.<sup>14</sup> Such a question has already been addressed by several groups<sup>1,14–17</sup> and very recently on bridging aryethynyl ligand<sup>18</sup> in binuclear ruthenium and iron complexes. In this study, we will focus on the noninnocent behavior of the dicyanamidobenzene BL. We report here the synthesis of  $[\{\text{Ru}(\text{tpy})(\text{thd})\}_2(\mu\text{-dicyd})]^+$ ,  $[\mathbf{3}][\text{PF}_6]$  with  $\text{tpy} = 2,2':6',2''\text{-terpyridine}$ ,  $\text{thd} = 2,2,6,6\text{-tetramethyl-3,5-heptanedione}$ , including the crystal structure in its +2 form, and the electrochemical and spectroscopic properties with detailed spectroelectrochemical studies over a wide range of accessible oxidation states as well as EPR and magnetic susceptibility measurements and computational investigations. The combination of all these studies gives some information on the frequently debated question for such systems: i.e. which is the oxidation site?

## 2. Results

**2.1. Synthesis.** The syntheses of **1** and **2** were adapted from literature procedures.<sup>19</sup> Mononuclear complex **2** could then be obtained from **1**. The chloride ligand is easily displaced by adding silver hexafluorophosphate in a refluxing

mixture of ethanol and water, and the resulting silver chloride precipitate can be eliminated by filtration. Addition of 10 equiv of 4-iodophenylcyanamide ligand led to complex **2** in a rather good yield (see Scheme 1).

Dinuclear complex  $[\mathbf{3}][\text{PF}_6]$  could be obtained via the same route (removal of the chloride ligand followed by complex-

(14) Ward, M. D.; McCleverty, J. A. *J. Chem. Soc., Dalton Trans.* **2002**, 3, 275.

(15) Bayly, S.; McCleverty, J. A.; Ward, M. D.; Gatteschi, D.; Totti, F. *Inorg. Chem.* **2000**, 39 (6), 1288. Bayly, S. R.; Humphrey, E. R.; de Chair, H.; Paredes, C. G.; Bell, Z. R.; Jeffery, J. C.; McCleverty, J. A.; Ward, M. D.; Totti, F.; Gatteschi, D.; Courric, S.; Steele, B. R.; Screttas, C. G. *J. Chem. Soc., Dalton Trans.* **2001**, 9, 1401. Chakraborty, S.; Laye, R. H.; Paul, R. L.; Gonnade, R. G.; Puranik, V. G.; Ward, M. D.; Lahiri, G. K. *J. Chem. Soc. Dalton Trans.* **2002**, 6, 1172. Chanda, N.; Laye, R. H.; Chakraborty, S.; Paul, R. L.; Jeffery, J. C.; Ward, M. D.; Lahiri, G. K. *J. Chem. Soc., Dalton Trans.* **2002**, 18, 3496. Meacham, A. P.; Druce, K. L.; Bell, Z. R.; Ward, M. D.; Keister, J. B.; Lever, A. B. P. *Inorg. Chem.* **2003**, 42 (24), 7887. Chanda, N.; Sarkar, B.; Fiedler, J.; Kaim, W.; Lahiri, G. K. *Dalton Trans.* **2003**, 18, 3550. Frantz, S.; Reinhardt, R.; Greulich, S.; Wanner, M.; Fiedler, J.; Duboc-Toia, C.; Kaim, W. *Dalton Trans.* **2003**, 17, 3370. Maurer, J.; Winter, R. F.; Sarkar, B.; Fiedler, J.; Zalis, S. *Chem. Commun.* **2004**, 17, 1900. Patra, S.; Sarkar, B.; Ghumaan, S.; Fiedler, J.; Kaim, W.; Lahiri, G. K. *Inorg. Chem.* **2004**, 43 (19), 6108. Patra, S.; Sarkar, B.; Ghumaan, S.; Fiedler, J.; Zalis, S.; Kaim, W.; Lahiri, G. K. *Dalton Trans.* **2004**, 5, 750. Ghumaan, S.; Sarkar, B.; Patra, S.; Parimal, K.; van Slageren, J.; Fiedler, J.; Kaim, W.; Lahiri, G. K. *Dalton Trans.* **2005**, 4, 706. Kar, S.; Sarkar, B.; Ghumaan, S.; Janardanan, D.; van Slageren, J.; Fiedler, J.; Puranik, V. G.; Sunoj, R. B.; Kaim, W.; Lahiri, G. K. *Chem. Eur. J.* **2005**, 11 (17), 4901. Kar, S.; Sarkar, B.; Ghumaan, S.; Roy, D.; Urbanos, F. A.; Fiedler, J.; Sunoj, R. B.; Jimenez-Aparicio, R.; Kaim, W.; Lahiri, G. K. *Inorg. Chem.* **2005**, 44 (24), 8715. Heilmann, M.; Frantz, S.; Kaim, W.; Fiedler, J.; Duboc, C. *Inorg. Chim. Acta* **2006**, 359 (3), 821. Patra, S.; Sarkar, B.; Maji, S.; Fiedler, J.; Urbanos, F. A.; Jimenez-Aparicio, R.; Kaim, W.; Lahiri, G. K. *Chem. Eur. J.* **2006**, 12 (2), 489.

ation of the dicyanamide bridging ligand) (see Scheme 1). Because the first oxidizing potential of the complex is very low ( $-0.24$  V versus SCE in  $\text{CH}_2\text{Cl}_2$ ,  $0.1$  M TBAHFP), after purification the complex is obtained in its mono-oxidized form as a hexafluorophosphate salt.

Chemical oxidation of the mononuclear complex **2** was performed in dichloromethane using ferrocenium hexafluorophosphate as an oxidizing agent. The corresponding hexafluorophosphate salt of the Ru(III) form of complex **2** was obtained. The possible excess of oxidizing agent could be easily removed by filtration through Celite, and the ferrocene side product was eliminated by precipitating the oxidized complex in a dichloromethane/cyclohexane mixture, filtering, and washing with cyclohexane.

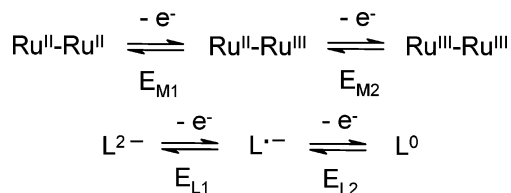
Chemical oxidation of the dinuclear complex  $[\mathbf{3}][\text{PF}_6]$  was also performed under the same conditions to obtain the dicationic form of the dinuclear complex.

**2.2. Electrochemistry.** Cyclic voltammograms (CVs) and differential pulse voltammograms (DPVs) of the complexes were recorded in dichloromethane, dimethylformamide, and/or acetonitrile under an argon atmosphere with  $0.1$  M tetrabutylammonium hexafluorophosphate (TBAH). The  $E_{1/2}$  potentials were determined from the average of the anodic and cathodic peak potentials for reversible waves. For irreversible waves, only the anodic peak potentials are reported.

The CV of complex **1** showed only one reversible wave in oxidation (at  $0.198$  V in dichloromethane and  $0.249$  V in dimethylformamide). This wave was assigned to the Ru(III/II) couple<sup>20</sup> and is slightly shifted toward the cathodic potentials compared to that of the equivalent complex  $[\text{Ru}(\text{tpy})(\text{acac})\text{Cl}]$  ( $0.288$  V in dimethylformamide) due to the addition of donor methyl groups on the acetylacetonate ligand.

The CV of complex **2** showed two waves in oxidation. The first quasireversible wave at  $0.200$  V corresponds to the Ru(III/II) couple. The second irreversible wave at  $1.064$  V was attributed to the oxidation of the cyanamide ligand.<sup>20,21</sup> This last point is consistent with the absence of this wave on the voltammogram of compound **1**, which does not contain this ligand.

The CV of dinuclear complex  $[\mathbf{3}][\text{PF}_6]$  presents three reversible waves in oxidation and one reversible wave in reduction (cf. Figures 1 and S1 and Table 1). Four redox couples can be considered: each metal can be reversibly oxidized once from Ru(II) to Ru(III), and the dicyanamido-benzene bridging ligand can also be reversibly oxidized twice<sup>7,9</sup> as shown:



This behavior is very similar to that of other complexes presenting the dicyanamidobenzene dianion as a bridging

(16) Kasack, V.; Kaim, W.; Binder, H.; Jordanov, J.; Roth, E. *Inorg. Chem.* **1995**, *34* (7), 1924.

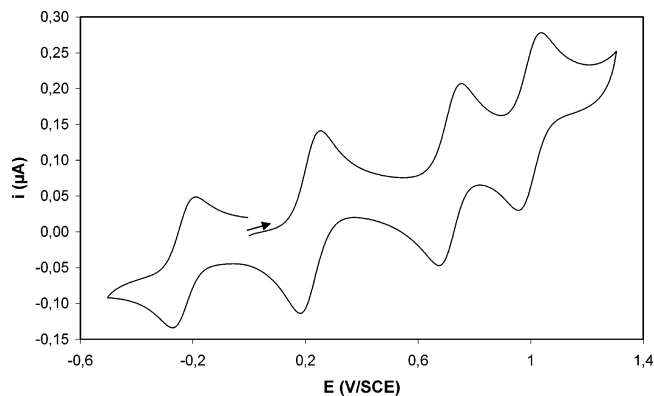


**Figure 1.** CV of complex  $[\mathbf{3}][\text{PF}_6]$ , platinum disk working electrode,  $0.1$  M TBAH in DCM, scan rate  $0.1$  V/s [scan Range:  $0.0 \rightarrow +1.3 \rightarrow -0.5 \rightarrow 0.0$  V].

ligand (see Table 1). Note that the potentials are anodically shifted when an amino group  $\text{NH}_3$  in  $[\{\text{Ru}(\text{NH}_3)_5\}_2(\mu\text{-dicyd})][\text{PF}_6]_4$  is replaced by  $\pi$ -acceptor ligands such as polypyridyl ligands. For complex **3**, containing a terpyridine ligand along with electron donor ligand thd, its potential should be expected to be intermediate between those of  $[\{\text{Ru}(\text{NH}_3)_5\}_2(\mu\text{-dicyd})][\text{PF}_6]_4$ <sup>12</sup> and  $[\{\text{Ru}(\text{tpy})(\text{bpy})\}_2(\mu\text{-dicyd})][\text{PF}_6]_2$ ,<sup>9</sup> as is actually the case.

**2.3. Electronic Absorption.** Electronic absorption data are summarized in Table 2. For  $\text{dicyd}^{2-}$ , spectroelectrochemical oxidation analysis was already done<sup>9</sup> but was reproduced here in DCM for the sake of comparison (see also Figure S2).

The spectra of complexes **1** and **2** in DCM showed two broad bands in the visible region (around  $570$  nm), which can be assigned to  $d\pi(\text{Ru}(\text{II})) \rightarrow \pi^*(\text{tpy})$  MLCT transitions.<sup>20</sup> The two intense bands (around  $280$  and  $320$  nm) are attributable to  $\pi \rightarrow \pi^*$  transitions of the terpyridine ligand.

Upon oxidation of complex **2**, the two broad bands around  $570$  nm disappeared, and a more intense band appeared at  $1005$  nm. This transition is absent in complex **1**<sup>+</sup>, which indicates that it implies the  $\text{Ipcyd}^-$  ligand. We assigned it to a  $\pi(\text{Ipcyd}) \rightarrow d\pi(\text{Ru}(\text{III}))$  LMCT transition. This was previously observed in oxidized complexes of the  $[\text{Ru}(\text{tpy})(\text{acac})]$  family.<sup>20</sup>

Dinuclear complex  $[\mathbf{3}][\text{PF}_6]$  also showed two broad bands around  $530$  nm which can be assigned to  $d\pi(\text{Ru}(\text{II})) \rightarrow \pi^*(\text{tpy})$  MLCT transitions and two intense bands (around  $280$  and  $320$  nm) which are attributable to  $\pi \rightarrow \pi^*$  transitions of the terpyridine ligand. These bands are almost twice as intense as the corresponding bands in the two mononuclear compounds, which is in agreement with the attribution proposed here. Complex  $[\mathbf{3}][\text{PF}_6]$  also presented an additional

(17) Sarkar, B.; Patra, S.; Fiedler, J.; Sunoj, R. B.; Janardanan, D.; Mobin, S. M.; Niemeyer, M.; Lahiri, G. K.; Kaim, W. *Angew. Chem., Int. Ed.* **2005**, *44* (35), 5655.

(18) Klein, A.; Lavastre, O.; Fiedler, J. *Organometallics* **2006**, *25* (3), 635.

(19) Dudd, L.; Hart, M.; Ring, D.; Sondaz, E.; Bonvoisin, J.; Coppel, Y. *Inorg. Chem. Commun.* **2003**, *6* (11), 1400. Slattery, S. J.; Bare, W. D.; Jameson, D. L.; Goldsby, K. A. *J. Chem. Soc., Dalton Trans.* **1999**, 1347.

(20) Fabre, M. A.; Jaud, J.; Bonvoisin, J. *J. Inorg. Chim. Acta* **2005**, *358* (7), 2384.

(21) Sondaz, E.; Gourdon, A.; Launay, J.-P.; Bonvoisin, J. *Inorg. Chim. Acta* **2001**, *316*, 79.

**Table 1.** Electrochemical Data<sup>a</sup>

species	E1	E2	E3	E4	ref
{Ru(NH <sub>3</sub> ) <sub>5</sub> } <sub>2</sub> (μ-dicyd)][PF <sub>6</sub> ] <sub>4</sub> <sup>b</sup>	-0.420	-0.134	0.565	0.997	12
{Ru(NH <sub>3</sub> ) <sub>4</sub> (py)} <sub>2</sub> (μ-dicyd)][PF <sub>6</sub> ] <sub>4</sub> <sup>b</sup>	-0.280	0.085	0.700	1.075	13
{Ru(NH <sub>3</sub> ) <sub>3</sub> (bpy)} <sub>2</sub> (μ-dicyd)][ClO <sub>4</sub> ] <sub>4</sub> <sup>b</sup>	-0.150	0.262	0.846	1.099	10
{Ru(tpy)(bpy)} <sub>2</sub> (μ-dicyd)][PF <sub>6</sub> ] <sub>2</sub> <sup>c</sup>	-0.015	0.425			9
[3][PF <sub>6</sub> ] <sup>c</sup>	-0.098	0.337	0.762		this work
[3][PF <sub>6</sub> ] <sup>b</sup>	-0.145	0.224	0.658	0.924	this work
[3][PF <sub>6</sub> ] <sup>d</sup>	-0.234	0.215	0.713	0.991	this work

<sup>a</sup> 0.1 M TBAH, 0.1 V/s, vs SCE. <sup>b</sup> In CH<sub>3</sub>CN. <sup>c</sup> In DMF. <sup>d</sup> In DCM.

**Table 2.** UV–Vis–NIR Absorption Data of the Investigated Compounds in DCM

species	absorption bands, λ in nm (ε 10 <sup>-3</sup> in M <sup>-1</sup> ·cm <sup>-1</sup> )					
<b>1</b>	281(28)	319(21)	407(8.1)		573(5.6)	666(4.5)
<b>1<sup>+</sup></b>	280(22)	309(18)	383(4.5)		590(1.8)	
<b>2</b>	281(40)	307(31)			574(5.5)	
<b>2<sup>+</sup></b>	265(38)	309(21)				1005(11)
<b>3</b>	276(81)	314(66)			588(12)	
<b>3<sup>1+</sup></b>	276(73)	314(57)	380(36)	530(14)		1366(25)
<b>3<sup>2+</sup></b>	274(77)	312(67)		472(13)		1290(54)
<b>3<sup>3+</sup></b>	274(69)	314(58)		436(11)	610(12)	1018(50)
<b>3<sup>4+</sup></b>	280(78)	318(66)			606(12)	
<b>dicyd<sup>2-</sup></b>	265(6.4)	294(13.6)				
	272(7.4)					
<b>dicyd<sup>-</sup></b>	265(7.5)	293(8.6)	362(4.1)		573(1.6)	620(3.0)
	272(7.7)					685(3.5)
<b>dicyd<sup>0</sup></b>	265(8.7)					
	272(7.6)					

transition at 380 nm, which we tentatively assigned to the dicyanamidobenzene bridging ligand, and a broad, intense and low energy transition at 1366 nm, the attribution of which will be discussed later.

**2.4. UV–Vis–NIR Spectroelectrochemistry.** Spectroelectrochemical studies of dinuclear complex [3][PF<sub>6</sub>] were performed in DCM (see Table 2) and also in acetonitrile and DMF to generate the spectra of the neutral form **3** and the charged forms **3<sup>2+</sup>**, **3<sup>3+</sup>**, and **3<sup>4+</sup>** of the dinuclear complex and are shown in Figure 2 (see also Figures S3–S6).

Upon reduction of dinuclear complex [3][PF<sub>6</sub>] to its neutral form, the broad and intense transition at 1366 nm disappears as well as the narrower transition at 380 nm.

During the electrochemical oxidation of dinuclear complex **3** from the charged form **3<sup>+</sup>** to the charged form **3<sup>2+</sup>**, the transition at 1366 nm is shifted toward higher energies (1290 nm) and the transition at 380 nm disappears.

During the electrochemical oxidation from the charged

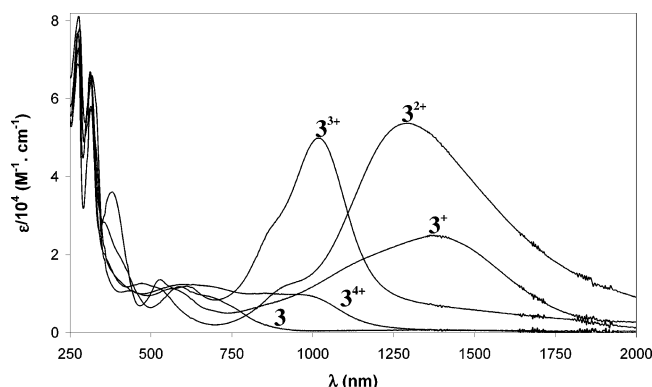


**Figure 2.** Spectroelectrochemical oxidation of **3** in DCM, 0.1M TBAH (see also Figures S3–S6).

form **3<sup>2+</sup>** to the charged form **3<sup>3+</sup>**, the transition at 1290 nm disappears and a thinner but as intense transition appears at 1018 nm.

During the electrochemical oxidation from the charged form **3<sup>3+</sup>** to the charged form **3<sup>4+</sup>**, the transition at 1018 nm disappears.

**2.5. EPR Spectra.** The EPR spectrum of [2][PF<sub>6</sub>] (see Figure S7) is a very typical rhombic spectrum of a low spin d<sup>5</sup> Ru(III) ion<sup>22</sup> with three well-resolved components:  $g_1 = 2.48$ ,  $g_2 = 2.13$ , and  $g_3 = 1.81$ . This gives the average  $g$  value of 2.16 ( $\langle g \rangle = [(g_1^2 + g_2^2 + g_3^2)/3]^{1/2}$ ) which is in very good agreement with the  $g$  value obtained by magnetic susceptibility measurements (see below). This average  $g$  value is a bit smaller than the one obtained for [Ru(tpy)-(acac)Ipcyd]<sup>+</sup> which is found to be 2.19 with  $g_1 = 2.55$ ,  $g_2 = 2.17$ ,  $g_3 = 1.79$ .<sup>23</sup> The smaller  $\langle g \rangle$  value for **3<sup>+</sup>** can be attributed to the stronger donor character of thd compared to acac as has already been observed on a series of dinuclear ruthenium complexes with various donor substituents.<sup>16</sup>

The EPR spectrum of [3][PF<sub>6</sub>] (Figure 3) showed the signal of an isotropic system with  $g = 2.02$  with a peak to peak separation of 60 G. This is characteristic of a radical species which indicates unique participation of the bridging ligand in the spin distribution.<sup>16,24</sup> This clearly rules out the [Ru<sup>II</sup>(μ-dicyd<sup>2-</sup>)Ru<sup>III</sup>] formulation and favors the radical one [Ru<sup>II</sup>(μ-dicyd<sup>-</sup>)Ru<sup>II</sup>] instead. One can also compare this

(22) Griffith, J. S. *The Theory of Transition-Metal Ions*; Cambridge University Press: London, 1961; p 363. Rieger, P. H. *Coord. Chem. Rev.* **1994**, *135–136*, 203.

(23) Sondaz, E. *Synthesis and Characterization of Cyanamide-Ruthenium complexes*. Ph.D. Thesis, Université Paul Sabatier-Toulouse III, Toulouse, 2001.

(24) Kaim, W.; Ernst, S.; Kasack, V. *J. Am. Chem. Soc.* **1990**, *112* (1), 173.

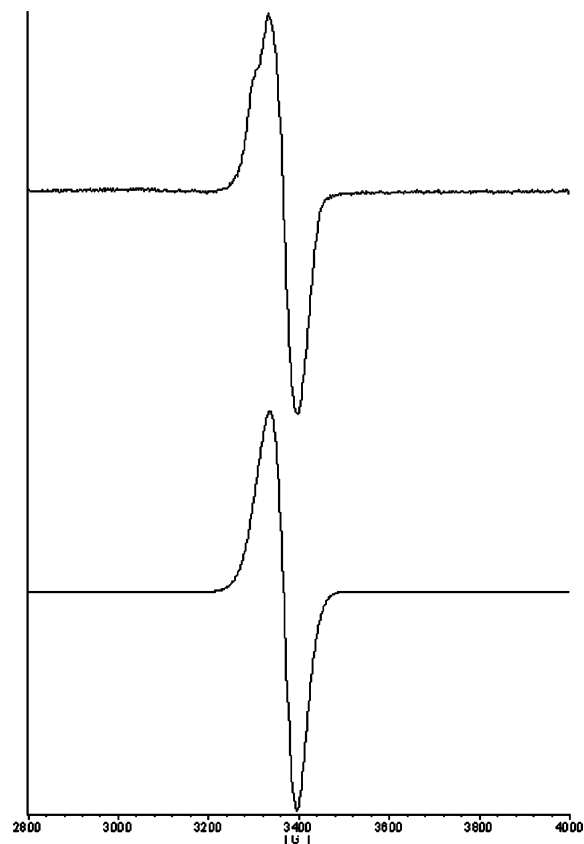


**Figure 3.** Experimental (top) EPR spectrum of  $3^+$  in frozen  $\text{CH}_2\text{Cl}_2$  (100 K) and simulated (bottom).

spectrum to the one observed for the potassium salt of dicyd $^{\cdot-}$ , which is centered at  $g = 2.0034$  and presents hyperfine coupling of around 1–5 G.<sup>25</sup> The spectrum observed for  $[3][\text{PF}_6]$  does not present any hyperfine coupling but is very similar to the one observed for the silver salt of DI-dicyd $^{\cdot-}$  (where DI-dicyd $^{\cdot-} = 2,5$ -diiodo-1,4-dicyanamidobenzene anion), where the absence of hyperfine coupling can be explained by interactions between the anion radical  $\pi$  system and the metallic d orbitals.<sup>26</sup>

The EPR spectrum of  $3^{3+}$  (Figure 4) showed the signal of an isotropic system with  $g = 2.08$  with a peak to peak separation of 290 G, which is 5 times broader than the signal of  $3^+$ .

**2.6. Magnetic Measurements.** We carried out variable-temperature (2–50 K) magnetic studies of powder samples of complexes  $2^+$  and  $3^+$ . The products of magnetic susceptibility ( $\chi$ ) with temperature ( $T$ ) versus  $T$  for both compounds are shown in Figure 5. Both compounds follow the Curie law down to 10 K. Below this temperature, the product ( $\chi T$ ) slightly decreases due to intermolecular antiferromagnetic interactions. Using the Curie–Weiss equation<sup>27</sup> (eq 1), we found  $g = 2.20$  and  $\theta = -0.40$  K for  $2^+$  and  $g = 1.95$  and  $\theta = -0.40$  K for  $3^+$ . Interestingly, the Curie constant for complex  $2^+$  was found to be  $C = 0.44 \text{ cm}^3 \cdot \text{mol}^{-1} \text{ K}$  ( $\mu_{\text{eff}} =$

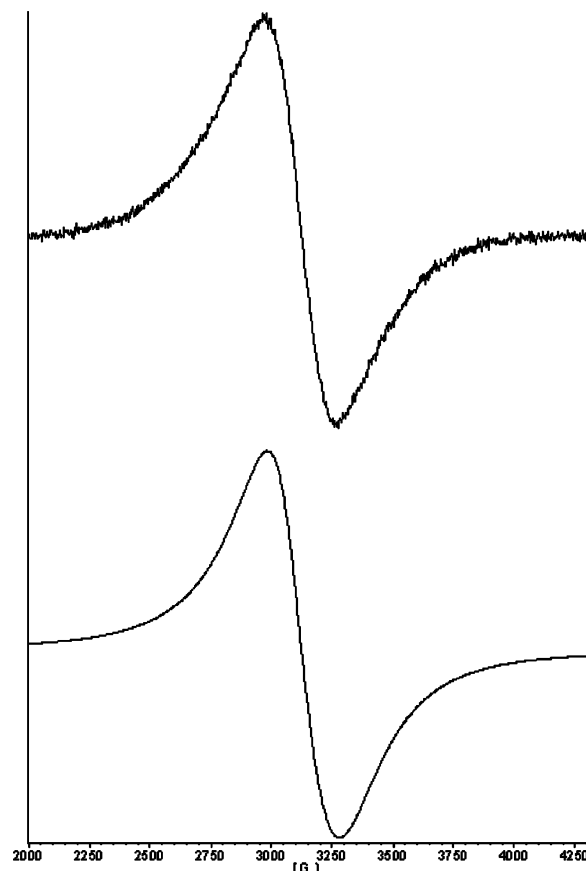


**Figure 4.** Experimental (top) EPR spectrum of  $3^{3+}$  in frozen  $\text{CH}_2\text{Cl}_2$  (100 K) and simulated (bottom).

$1.88 \mu_{\text{B}}$ ), which is very typical of a low spin ruthenium(III)  $S = 1/2$  state,<sup>28</sup> and for complex  $3^+$  we found  $C = 0.35 \text{ cm}^3 \cdot \text{mol}^{-1} \text{ K}$  ( $\mu_{\text{eff}} = 1.67 \mu_{\text{B}}$ ), which is much closer to a typical radical  $S = 1/2$  state with  $g = 2.0$ ,  $C = 0.375 \text{ cm}^3 \cdot \text{mol}^{-1} \text{ K}$ , and  $\mu_{\text{eff}} = 1.732 \mu_{\text{B}}$ .

$$\chi_{\text{M}} = \frac{Ng^2\mu_{\text{B}}^2S(S+1)}{3k(T-\theta)} \quad (1)$$

**2.7. X-ray Crystallography.** The ORTEP diagram of complex  $[3][\text{PF}_6]_2$  is shown in Figures 6 and 7. The hexafluorophosphate counteranions were omitted for the sake of clarity. Crystallographic data are shown in Table 3, and selected bond lengths and angles are given in Supporting Information. The particularity of this structure is the presence of two independent molecules, conformers A (Figure 6) and B (Figure 7). The cyanamide groups are in an anti configuration as has already been seen in similar systems.<sup>7,10</sup> Each of these two molecules is centrosymmetric with a center of symmetry on the central phenyl ring of the bridging ligand. Their structures are very similar. This led us to check the accuracy of the space group by the use of PLATON, which confirmed that the chosen group was the good one. There are two types of  $3^{2+}$  in the unit cell (conformers A and B), which crystallized on two symmetry positions; as  $Z = 8$ , this makes  $4 + 4 = 8$  complexes  $3^{2+}$  per unit cell. There are

(25) Gerson, F.; Gescheidt, G.; Möckel, R.; Aumüller, A.; Erk, P.; Siegfried, H. *Helv. Chim. Acta* **1988**, *71*, 1665.

(26) Mori, T.; Inokuchi, H.; Kobayashi, A.; Kato, R.; Kobayashi, H. *Phys. Rev. B* **1988**, *38*, 5913. Sakurai, T.; Nakagawa, N.; Okubo, S.; Ohta, H.; Kanoda, K.; Hiraki, K. *J. Phys. Soc. Jpn.* **2001**, *70* (6), 1794.

(27) O'Connor, C. J. *Prog. Inorg. Chem.* **1982**, *29*, 203.

(28) Figgis, B. N.; Lewis, J.; Mabbs, F. E.; Webb, G. A. *J. Chem. Soc. (A)* **1966**, 422.

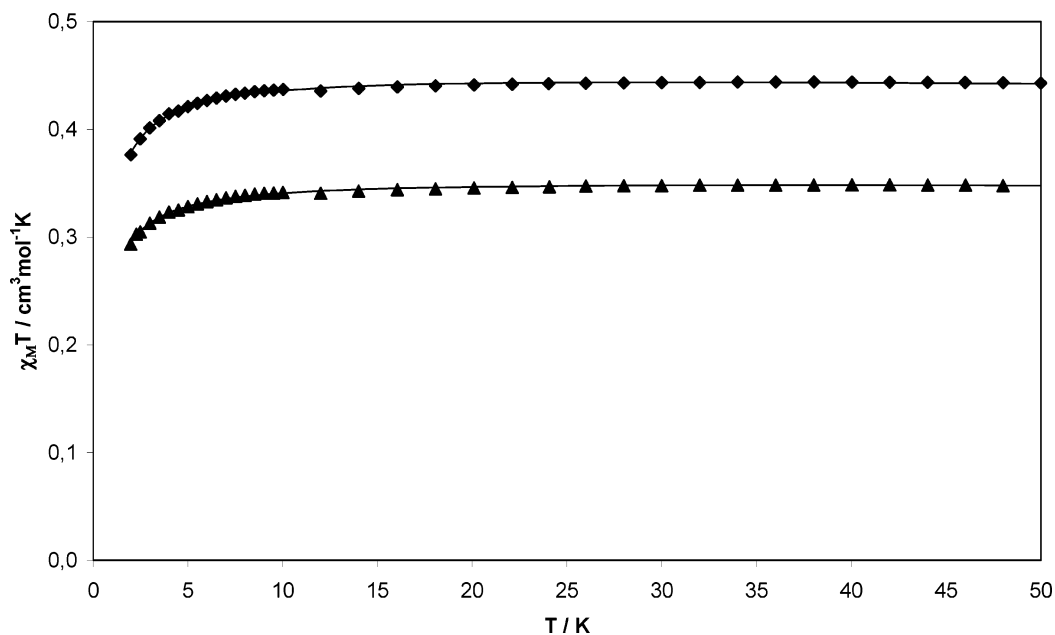


Figure 5.  $\chi_M T$  versus  $T$  recorded on powder samples of  $[2][PF_6]$  (■) and  $[3][PF_6]$  (▲) and theoretical laws according to eq 1.

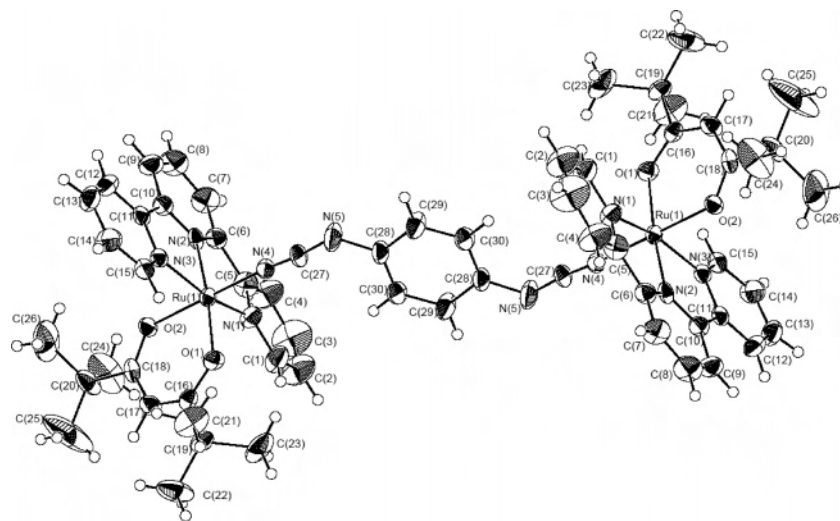


Figure 6. ORTEP drawing of complex  $[3][PF_6]_2$  (conformer A) along with the atom numbering scheme, probability level of 30%.

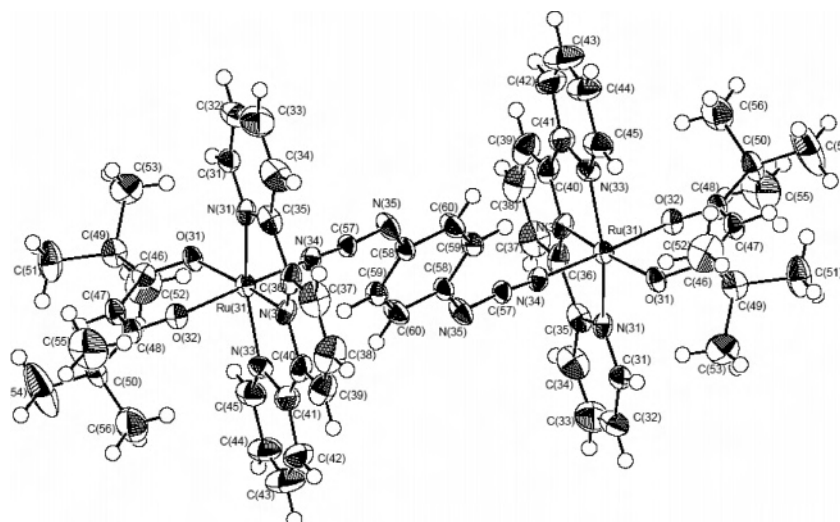


Figure 7. ORTEP drawing of complex  $[3][PF_6]_2$  (conformer B) along with the atom numbering scheme, probability level of 30%.

**Table 3.** Crystallographic Data and Refinement Parameters for [3][PF<sub>6</sub>]<sub>2</sub>

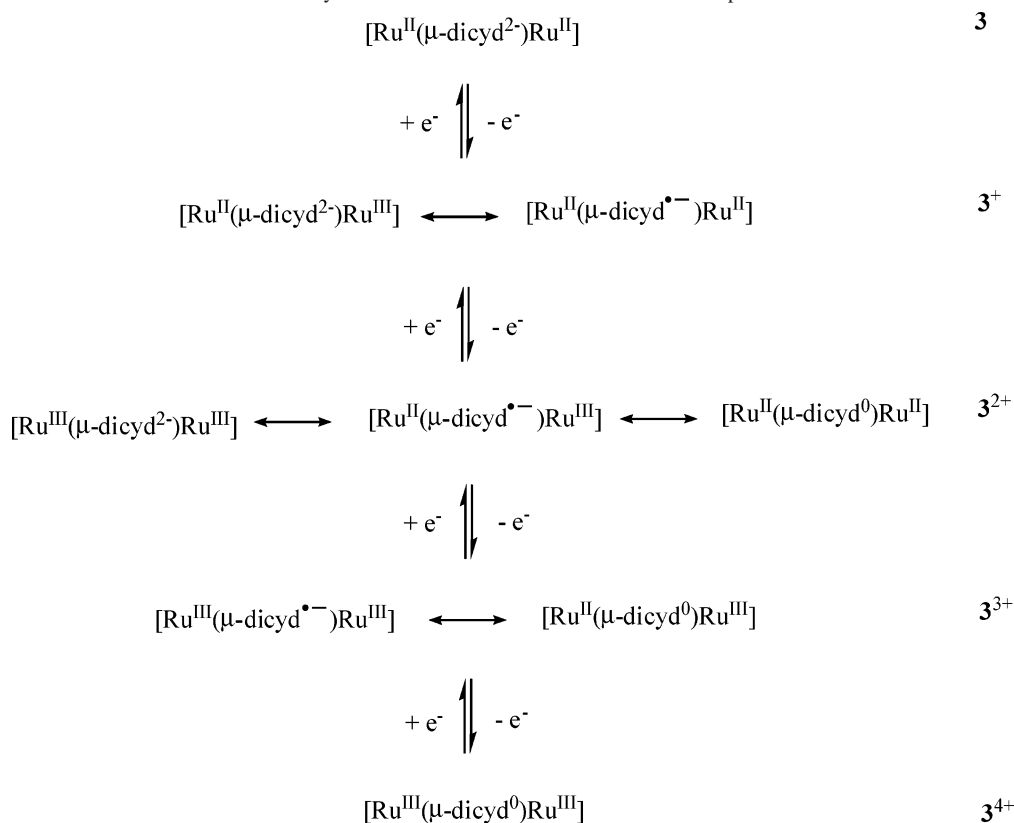
formula	C <sub>60</sub> H <sub>64</sub> F <sub>12</sub> N <sub>10</sub> O <sub>4</sub> P <sub>2</sub> Ru <sub>2</sub>
cryst syst	monoclinic
fw (g mol <sup>-1</sup> )	1481.3
space group	C2/c
a, Å	27.246(2)
b, Å	30.008(2)
c, Å	20.150(2)
β, deg	107.960(9)
V, Å <sup>3</sup>	15672(2)
Z	8
μ(Mo Kα) (mm <sup>-1</sup> )	0.499
ρ <sub>calcd</sub> (g cm <sup>-3</sup> )	1.256
2θ max (deg)	28
no. total reflns	17767
no. unique reflns with I > 2σ(I)	4313
abs correction	multiscan
T <sub>min</sub> /max	0.615/0.917
R <sub>f</sub> <sup>a</sup>	0.0665
R <sub>w</sub> <sup>b</sup>	0.174
GOF	0.902

$$^a R_f = \sum ||F_o| - |F_c|| / \sum |F_o|. \quad ^b R_w = (\sum w|F_o| - |F_c|)^2 / \sum w|F_o|^2)^{1/2}.$$

three types of PF<sub>6</sub><sup>-</sup>, one type lies on a general position and the two other types lie on two symmetry positions, which makes 8 + 4 + 4 = 16 PF<sub>6</sub><sup>-</sup> per unit cell (see Figure S8).

### 3. Discussion

The cyclic voltammogram of dinuclear complex [3][PF<sub>6</sub>] presents three reversible waves in oxidation and one reversible wave in reduction. Four redox couples can be considered: each metal can be reversibly oxidized once from Ru(II) to Ru(III), and the dicyanamidobenzene bridging ligand (dicyd<sup>2-</sup>) can also be reversibly oxidized twice to form a radical anion species (dicyd<sup>•-</sup>) and a neutral species (dicyd<sup>0</sup>).

**Scheme 2.** Various Electronic Structures Which May Be Used to Describe the Oxidation of Compound 3

To sum up, dinuclear complex **3** presents four reversible waves in electrochemistry, and four redox couples can be considered. The title complex was obtained in its mono-oxidized form, but for pedagogical purposes, it is clearer to start from the fully reduced **3**<sup>0</sup> species and look at its behavior upon progressive oxidation. The question is which part of the complex is oxidized first? How can we assign each redox couple to each wave? If one looks at every possible electronic structure for each oxidation step, one notices that this is a complicated system with a very rich behavior in oxidation (Scheme 2).

Note that the highest complexity occurs for the intermediate oxidation state **3**<sup>2+</sup>, for which three different electronic structures can be written.

To answer the difficult problem of the site of oxidation, we have analyzed the experimental results along with the theoretical ones. Calculations were performed for the first three members of the series, i.e., **3**, **3**<sup>+</sup>, and **3**<sup>2+</sup>. There are several ways to answer this question using the output of DFT calculations: (i) using the variation of atomic charges, computed according to either Mulliken or Lowdin rules, (ii) using the spin densities, in the case of an open shell system such as **3**<sup>+</sup>, and (iii) using molecular orbital diagrams and the correlation from one compound to the other. Method iii is in principle less satisfactory since the DFT method does not rely on the concept of molecular orbitals and is actually designed to deal with the total charge density.

**3.1. Neutral Complex 3.** In its neutral form, the dinuclear complex presents formally two ruthenium(II) centers linked to two neutral tpy ligands, two anionic thd ligands, and a

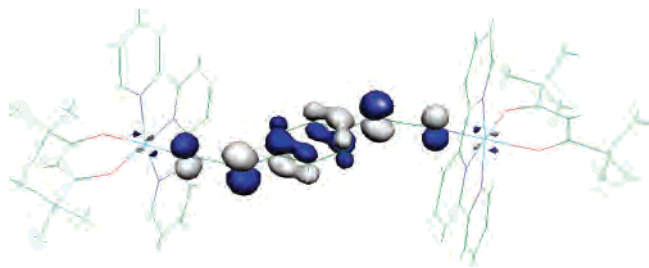


Figure 8. Highest occupied molecular orbital (HOMO) for complex **3**.

dianionic bridging ligand dicyd<sup>2-</sup>. Upon reduction of dinuclear complex **[3][PF<sub>6</sub>]** to its neutral form **3<sup>0</sup>**, the characteristic UV–vis spectrum of a Ru(II) complex is recovered, with two broad bands in the visible region, which can be assigned to  $d\pi(\text{Ru(II)}) \rightarrow \pi^*(\text{tpy})$  MLCT transitions. The ground state of the complex is thus a closed shell singlet. The HOMO of the complex (Figure 8) is predominantly localized on the bridging ligand dicyd, with a contribution of 89%. This first result is in favor of the oxidation of the bridging ligand before the oxidation of the metal, as shown experimentally by the EPR spectrum of complex **3<sup>+</sup>**. Of course, one has to be careful with conclusions drawn from the sole inspection of the HOMO, because orbital reorganization can occur once the complex is oxidized. But this conclusion is supported by calculations on the mono-oxidized form (see below).

Interestingly, the structure of the bridging ligand in complex **3** is very similar to the optimized geometry of the free dicyd<sup>2-</sup> ligand, the largest deviation for the computed bond lengths a, b, c, and d being only 0.01 Å. This indicates that the benzenic ring of the ligand is almost unchanged upon complexation.

**3.2. Mono-Oxidized Form 3<sup>+</sup>.** If the metal was oxidized first, **3<sup>+</sup>** could be the mixed-valence form of the complex (Ru<sup>II</sup>–dicyd<sup>2-</sup>–Ru<sup>III</sup>). The broad, intense and low energy transition at 1366 nm on the electronic absorption spectrum could then be attributed to an intervalence transition. On the other hand, if the ligand is oxidized first (Ru<sup>II</sup>–dicyd<sup>•-</sup>–Ru<sup>II</sup>), this transition could be a  $d\pi(\text{Ru(II)}) \rightarrow \pi^*(\text{dicyd}^{\bullet-})$  metal to ligand charge transfer transition (MLCT). One could object that if the ligand is oxidized first, one should observe the radical anion chromophore which presents four bands in the range 300–700 nm,<sup>9</sup> but these bands are probably masked by the above-described MLCT transitions which are 4 or 5 times more intense (see Figure S2). Here, the electronic absorption spectrum is not enough to draw a conclusion.

However, the EPR spectrum of **[3][PF<sub>6</sub>]** showed the signal of an isotropic system with  $g = 2.02$ . This is very characteristic of a radical species, which seems to indicate that the radical anion form of the bridging ligand is preferred, which means that the ligand is oxidized first. Moreover, supposing the metal would be oxidized first to form a mixed-valence species, it has to be remembered that even a class III mixed-valence complex would keep the characteristics of Ru(III), that is to say a rhombic signal.<sup>29</sup> This should be

(29) Stebler, A.; Ammeter, J. H.; Furholz, U.; Ludi, A. *Inorg. Chem.* **1984**, *23*, 2764.

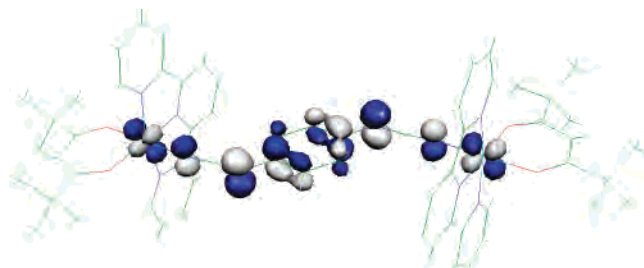


Figure 9. Singly occupied molecular orbital (SOMO) for complex **3<sup>+</sup>**.

true whatever the transfer mechanism is (ET or HT). There is then evidence that the ligand is oxidized first. Magnetic susceptibility measurement is completely in agreement with this point showing an effective magnetic moment much closer to a radical  $S = 1/2$  spin state with  $g$  close to 2.0, rather than a ruthenium(III) low spin  $S = 1/2$  which would have a larger  $g$  value close to  $g = 2.2$ . Other examples of radical anions as ligands<sup>30</sup> can be found in the literature, but they are rather scarce as bridging ligands.<sup>16,17,24</sup>

For the theoretical study of **3<sup>+</sup>**, a full geometry optimization was performed at the unrestricted Hartree–Fock level (UHF). The spin contamination was found to be negligible with  $\langle S^2 \rangle = 0.764$ , which differs from the theoretical value  $\langle S^2 \rangle = S(S + 1) = 0.750$  by less than 2%.

In a comparison of the structure of the bridging ligand in complex **3<sup>+</sup>** to the computed structure of the radical anion, L<sup>•-</sup> shows only very slight differences, the largest deviation for the computed bond lengths a, b, c, and d being only 0.004 Å. The evolution of the atomic charges shows the same trend, with a charge 1+ distributed mainly on the bridging ligand (59%), the two tpy ligands (28%), and the two thd ligands (14%).

The presence of an anion radical bridging ligand is also supported by the computed total spin density on the bridging ligand, which amounts to 0.90, clearly indicating that the bridging ligand was oxidized while the two ruthenium centers remained essentially untouched.

Looking now at the molecular orbitals, since the calculations are performed in a self-consistent way on the oxidized form, the shape of the SOMO carries also some information on the site where oxidation has occurred. As shown in Figure 9, the SOMO resembles the HOMO of **3**, in agreement with a ligand-based oxidation. However, it has to be noticed that the proportion of the bridging ligand in this orbital, though still very significant (74%), has slightly decreased upon oxidation (cf. 89% in the HOMO of **3**).

**3.3. Dioxidized Form 3<sup>2+</sup>.** The electrochemical oxidation of **3<sup>+</sup>** to the dioxidized form **3<sup>2+</sup>** followed by electronic absorption spectroscopy shows that the main transition is shifted toward higher energies and is also more intense. Again, the electronic absorption spectrum does not enable

(30) Kaim, W. *Coord. Chem. Rev.* **1987**, *76*, 187. Bhattacharya, S.; Gupta, P.; Basuli, F. *Inorg. Chem.* **2002**, *41*, 5810. Chaudhuri, P.; Verani, C. N.; Bill, E.; Bothe, E.; Weyhermueller, T.; Wieghardt, K. *J. Am. Chem. Soc.* **2001**, *123* (10), 2213. Herebian, D.; Wieghardt, K. E.; Neese, F. *J. Am. Chem. Soc.* **2003**, *125* (36), 10997. Herebian, D.; Bothe, E.; Neese, F.; Weyhermueller, T.; Wieghardt, K. *J. Am. Chem. Soc.* **2003**, *125* (30), 9116.



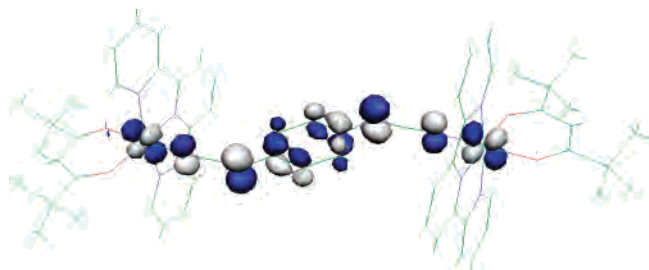


**Figure 10.** Lowest unoccupied molecular orbital (LUMO) for complex  $3^{2+}$ .

us to conclude on the nature of this oxidation. Should the electronic structure of  $3^{2+}$  be  $\text{Ru}^{\text{II}}-\text{dicyd}^0-\text{Ru}^{\text{II}}$ , this transition could be assigned to a  $d\pi(\text{Ru}(\text{II})) \rightarrow \pi^*(\text{dicyd}^0)$  MLCT transition. Now, supposing the electronic structure is  $\text{Ru}^{\text{II}}-\text{dicyd}^{\cdot-}-\text{Ru}^{\text{III}}$ , we could attribute this transition to an intervalence transition. The dioxidized form  $3^{2+}$  is EPR silent, which is compatible with both electronic structures.  $\text{Ru}^{\text{II}}-\text{dicyd}^0-\text{Ru}^{\text{II}}$  is clearly diamagnetic whereas in the case of  $\text{Ru}^{\text{II}}-\text{dicyd}^{\cdot-}-\text{Ru}^{\text{III}}$  the absence of signal in EPR could be interpreted by a strong antiferromagnetic coupling between the Ru(III) ion and the anion radical ligand (or between the two Ru(III) ions for  $\text{Ru}^{\text{III}}-\text{dicyd}^{2-}-\text{Ru}^{\text{III}}$ ).

The ground state of the EPR-silent complex  $3^{2+}$  might, in principle, be either a closed shell singlet or an antiferromagnetically coupled open shell singlet. We performed the calculation assuming it was a closed shell singlet.

The computed structural parameters of complex  $3^{2+}$  in its closed shell singlet state at the B3LYP level of theory are found to be in good agreement with the corresponding values obtained from the X-ray structure. The largest deviations between experimental and computed bond lengths and angles are only about 0.07 Å and 3.6°, respectively.

The optimized structure shows that the geometry of the bridging ligand is intermediate between the optimized geometries of the two forms  $\text{L}^{\cdot-}$  and  $\text{L}^0$  of the free ligand, but rather closer to the geometry of the radical anionic form. Another argument in favor of the oxidation of the metal is the shortening of the metal–ligand bond (g) by 0.05 Å from complex  $3^+$  to complex  $3^{2+}$ . This trend may be explained on an electrostatic point of view. Assuming the oxidation from  $3^+$  to  $3^{2+}$  is based on the metal, the charge on the bridging ligand is then unchanged (1<sup>-</sup>), whereas the formal charges on the two metals increase from 2<sup>+</sup> to 2.5<sup>+</sup>. One should then expect the attraction between the metal and the ligand to increase and the length of the metal–ligand bond to decrease. On the other hand, if the ligand was oxidized once more at this stage, its charge would change from 1<sup>-</sup> to 0 whereas the formal charges on the metals would remain the same. This should end up in a lengthening of the metal–ligand bond, which is not the case.

Examining the evolution of the atomic charges shows that the 2<sup>+</sup> charge is distributed half on the bridging ligand (46–50%) and half on the  $[\text{Ru}(\text{tpy})(\text{thd})]$  moiety (50–52%), which would be in favor of a metal centered oxidation.

Regarding molecular orbitals, the LUMO of complex  $3^{2+}$  resembles at first sight the SOMO of  $3^+$  and the HOMO of  $3$  (see correlation diagram of Figure 13), suggesting that

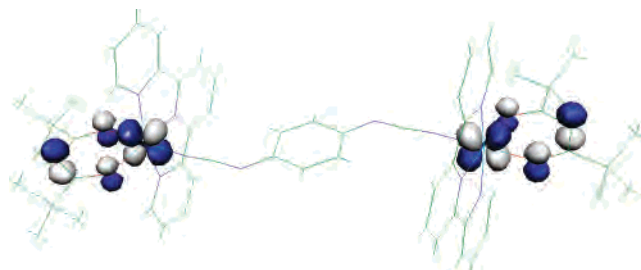


**Figure 11.** Highest occupied molecular orbital (HOMO) for complex  $3^{2+}$ .

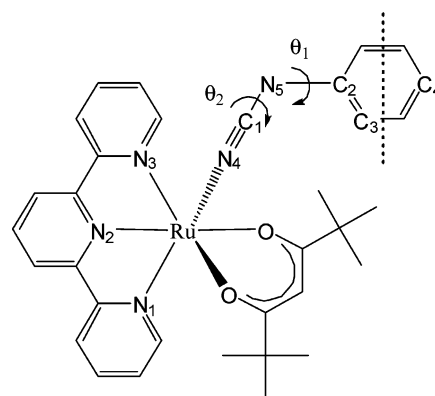


**Figure 12.** Degrees of freedom of the dinuclear complex. Two possible rotation angles,  $\theta_1$  and  $\theta_2$ , can be identified on each moiety.

oxidation has occurred here. However, the LUMO of  $3^+$  (Figure 10) exhibits a decreased contribution from the ligand (70%) and an increased contribution from the two ruthenium atoms (18%), showing some tendency to oxidize the metal(s). The HOMO mainly implies the ruthenium moieties (Figure 11), with 43% on the ruthenium atoms, 43% on the thd ligands, and only 9% on the bridging ligand. The composition of the LUMO (Figure 10) does not enable us to conclude clearly as it shows that the second oxidation occurred half on the bridging ligand (40%) and half on the  $[\text{Ru}(\text{tpy})(\text{thd})]$  moiety (60%).

To sum up, the determination of the oxidation site from  $3^+$  to  $3^{2+}$  is not so clear as for the first oxidation, and a ruthenium-based oxidation, as we tentatively assumed from the experimental data, is possible. Note that the present calculations are valid for isolated molecules (gas phase) while the experimental study is made in solution. This could explain why experimental and theoretical results are not in complete agreement.

Here, the X-ray structure of  $3^{2+}$  can give good pieces of information concerning the electronic structure. One can compare the structure of the coordinated ligand to the structure of its free dianionic form  $\text{dicyd}^{2-}$  and of its free neutral form  $\text{dicyd}^0$ . It is interesting to notice that upon oxidation of  $\text{dicyd}^{2-}$  to  $\text{dicyd}^0$ , the structure of the ligand changes from a benzenic form to a quinonic form: one can observe a shortening of bonds b (C–C) and d (C–N) and a lengthening of bonds a and c (C–C) (see Scheme 3 and Table 4). In a comparison of a few bond lengths, the structure of the coordinated ligand in complex  $3^{2+}$  appears to be halfway between the free dianionic form  $\text{dicyd}^{2-}$  and the free neutral form  $\text{dicyd}^0$ , which seems to indicate that the coordinated ligand is in its mono-oxidized form  $\text{dicyd}^{\cdot-}$  in dinuclear

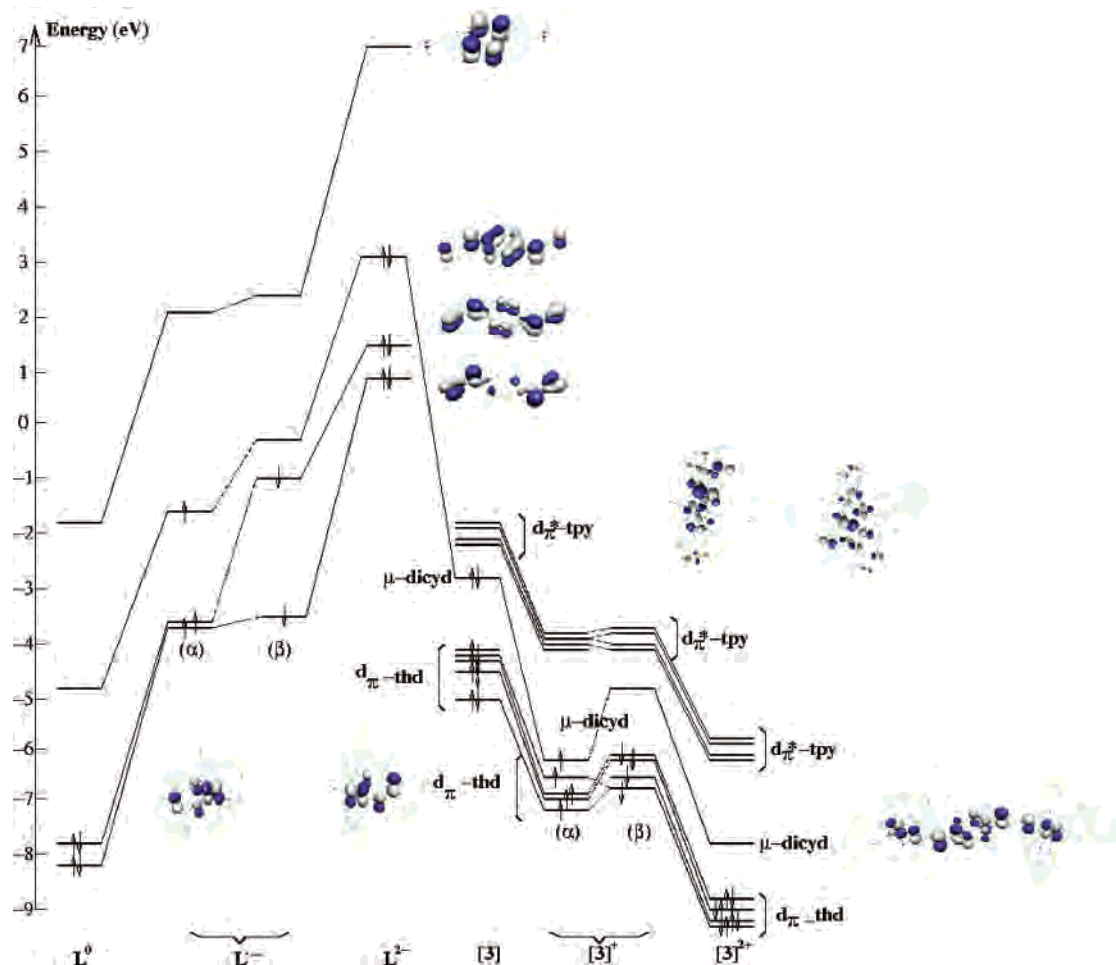
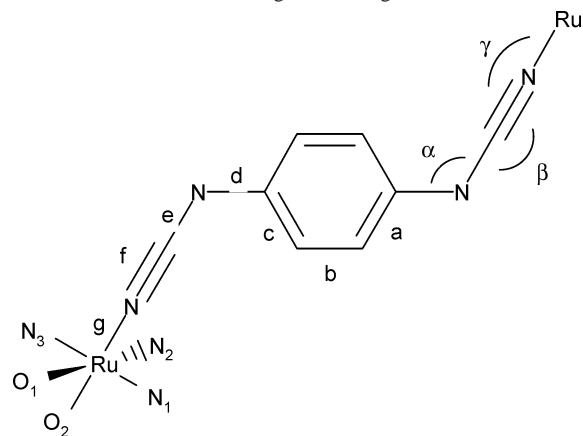
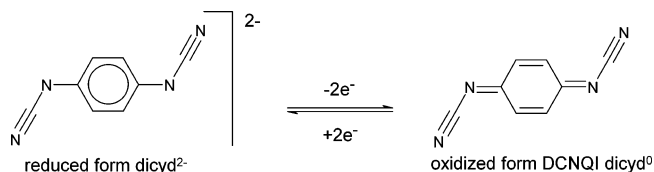


**Figure 13.** Frontier molecular orbitals correlation diagram for bridging ligand **L** and binuclear complex **3** in their first three oxidized states.

**Scheme 3.** Pertinent Bond Lengths and Angles



complex  $3^{2+}$ . This structure is intermediate between the benzenic structure of the dianion  $\text{dicyd}^{2-}$  and the quinonic structure of DCNQI ( $\text{dicyd}^0$ ) as shown for  $\text{dicyd}^{\bullet-}$  salts with porphyrinatomanganese(II).<sup>31</sup>



This would be a nice example of a mixed-valence system where the electronic interaction would occur through a radical anionic ligand.

**3.4. Tri- and Tetraoxidized Torms  $3^{3+}$  and  $3^{4+}$ .** Upon further oxidation from  $3^{2+}$  to  $3^{3+}$ , the transition at 1290 nm disappears, and a sharper transition appears at 1018 nm. The shape and the energy of this transition are similar to that of LMCT transitions observed for Ru(III) mononuclear complexes; the electronic structure of  $3^{3+}$  would then appear to be  $\text{Ru}^{\text{III}}-\text{dicyd}^{\bullet-}-\text{Ru}^{\text{III}}$ . This transition could then be attributed to a  $\pi(\text{dicyd}^{\bullet-}) \rightarrow d\pi(\text{Ru}(\text{III}))$  LMCT transition.

The EPR of  $3^{3+}$  shows a broad and isotropic signal centered on  $g = 2.08$ . This is neither characteristic of a radical species (in which case the signal should be sharp and centered on 2.00) nor of a low spin Ru(III) ion (which is a rhombic system). However, assuming the electronic structure of  $3^{3+}$  to be  $\text{Ru}^{\text{III}}-\text{dicyd}^{\bullet-}-\text{Ru}^{\text{III}}$ , the EPR spectrum could be interpreted as the signal of an effective spin  $1/2$  resulting from the interaction of three highly coupled spins  $1/2$  (carried by two Ru(III) ions and the anion radical  $\text{dicyd}^{\bullet-}$ ).

This is coherent with what can be observed during the oxidation from  $3^{3+}$  to  $3^{4+}$  followed by spectroelectrochemistry. During this step, the ligand is oxidized from  $\text{dicyd}^{\bullet-}$

(31) Sugiura, K.; Mikami, S.; Johnson, M. T.; Raebiger, J. W.; Miller, J. S.; Iwasaki, K.; Okada, Y.; Hino, S.; Sakata, Y. *J. Mater. Chem.* **2001**, *11*, 2152.

**Table 4.** Experimental Data for Selective Bond Lengths and Angles

	DCNQI	[AsPh <sub>4</sub> ] <sub>2</sub> [dicyd]	3 <sup>2+</sup> (A)	3 <sup>2+</sup> (B)	[{Ru(NH <sub>3</sub> ) <sub>5</sub> } <sub>2</sub> (μ-dicyd)] [TsO] <sub>4</sub> <sup>a</sup>	[{mer-Ru(bpy)(NH <sub>3</sub> ) <sub>3</sub> } <sub>2</sub> (μ-dicyd)] [ClO <sub>4</sub> ] <sub>4</sub> <sup>b</sup>	[Mn <sup>III</sup> TMesP] <sup>+</sup> [DMeDCNQI] <sup>•-c</sup>	[Mn <sup>III</sup> TMesP] <sup>+</sup> [DMeDCNQI] <sup>•-d</sup>
<i>a</i> /Å	1.446(2)	1.398(8)	1.410(13)	1.402(12)	1.406(20)	1.440(14)–1.444(14)	1.435(6)	1.437(3)
<i>b</i> /Å	1.336(2)	1.385(9)	1.359(13)	1.348(12)	1.386(20)	1.348(14)–1.355(14)	1.352(5)	1.364(3)
<i>c</i> /Å	1.450(2)	1.399(9)	1.396(14)	1.418(11)	1.386(20)	1.426(14)–1.426(14)	1.428(6)	1.411(3)
<i>d</i> /Å	1.303(2)	1.388(8)	1.335(12)	1.350(10)	1.376(17)	1.331(12)–1.335(13)	1.359(5)	1.350(3)
<i>e</i> /Å	1.334(2)	1.299(10)	1.280(12)	1.287(10)	1.298(19)	1.309(14)–1.316(14)	1.309(6)	1.306(3)
<i>f</i> /Å	1.150(2)	1.172(10)	1.152(11)	1.154(10)	1.151(19)	1.162(13)–1.172(12)	1.163(6)	1.156(3)
<i>g</i> /Å			1.966(6)	1.969(6)	1.938(11)	1.978(8)–1.977(9)	2.261(4)	2.249(2)
$\alpha$ /deg	119.5(2)	118.7(5)	124.4(8)	124.0(7)	119.7(12)	121.3(9)–122.6(9)		
$\beta$ /deg	172.8(2)	174.1(6)	173.9(10)	173.2(8)	171.5(15)	169.2(10)–173.9(11)	173.1(4)	175.9(2)
$\gamma$ /deg			174.0(7)	173.3(6)	175.1(10)	174.1(8)–178.1(8)	158.4(4)	150.7(2)
<i>T</i> (K)		295	298	298	295	298		223
ref	46	47	this work	this work	7	10	31	31

<sup>a</sup> Conformer A. <sup>b</sup> Not centrosymmetric. <sup>c</sup> *meso*-Tetrakis(2,4,6-trimethylphenyl)porphyrinatomanganese(III) 2,5-dimethyl-*N,N'*-dicyanoquinone diimine. <sup>d</sup> *meso*-Tetrakis(2,4,6-trimethoxyphenyl)porphyrinatomanganese(III) 2,5-dimethyl-*N,N'*-dicyanoquinone diimine.

to dicyd<sup>0</sup>, which causes the disappearance of the  $\pi(\text{dicyd}^{\bullet-}) \rightarrow d\pi(\text{Ru(III)})$  LMCT transition at 1018 nm.

#### 4. General Conclusion

Multiple spectroscopic, electrochemical, and spectroelectrochemical investigations have revealed the influence of the dicyanamidobenzene bridging ligand system on the intramolecular electron transfer abilities of binuclear ruthenium complexes.

We have attempted to establish the oxidation state distribution for the various accessible redox states of compound **3**, using a combination of UV–vis–NIR and spectroelectrochemistry. Theoretical calculations at the DFT level for **3**, **3**<sup>+</sup>, and **3**<sup>2+</sup> were also helpful and are in general agreement with experimental data.

The following has been shown in this work: (a) The dicyanamido ligand is a truly “noninnocent” bridging ligand and is oxidized first. (b) Then, one of the Ru(II) ions is oxidized next to form a Ru<sup>II</sup>–dicyd<sup>•-</sup>–Ru<sup>III</sup> system which would possibly be one of the rare examples<sup>17</sup> of an unconventional mixed-valent system where the electronic interaction occurs through an open shell anion radical ligand and a new class of singlet species composed from metal/ligand/metal intramolecular spin–spin coupling. At the present stage, it is not possible to know if the mixed valence is localized (class II) or delocalized (class III) according to Robin and Day classification.<sup>32</sup> (c) The third oxidation produced the Ru<sup>III</sup>–dicyd<sup>•-</sup>–Ru<sup>III</sup> system where metal- and ligand-based spins have a strong antiferromagnetic interaction, leading to a net effective  $S = 1/2$  resultant spin state. This would then open the possibility of studying both the electro- and the magnetocommunication in the same system soon.

One may notice that a simple electrostatic argument may be evoked to explain the order of these oxidations, once recognizing that the first site of oxidation, starting from **3**, is the dicyanamido ligand. If the ligand is oxidized first, it will be difficult to oxidize it once more. The metal is thus oxidized next and then the other metal, which is farther from the first oxidized metal than the ligand. Finally, the ligand

is oxidized to the neutral state at the end, when there is no other choice.

The first goal of this study was to look for a mixed-valent system with a good electronic communication. The dicyanamidobenzene ligand was supposed to be well-suited to mediate metal–metal interactions because of the close proximity in energy of its HOMO with the metal orbitals. By this very fact, we have found a more complicated system, full of potential, i.e., the capability to finely modulate the interaction between the two metals with slight modifications of the bridging ligand or of the ancillary ligands.

#### 5. Experimental Section

**5.1. Materials.** All chemicals and solvents were reagent grade or better. [Ru(tpy)Cl<sub>3</sub>],<sup>33</sup> IpcydH,<sup>21</sup> dicydH<sub>2</sub>,<sup>7</sup> and [AsPh<sub>4</sub>]<sub>2</sub>[dicyd]<sup>7,9</sup> were prepared according to literature procedures. Weakly acidic Brockmann I type alumina (Aldrich) was used.

**5.2. Physical Measurements.** UV–vis spectra were recorded on a Shimadzu UV-3100 spectrophotometer. <sup>1</sup>H and <sup>13</sup>C NMR spectra were recorded on a Bruker AMX-500 in CD<sub>2</sub>Cl<sub>2</sub>. IR spectra of samples in KBr pellets were taken on a Perkin-Elmer 1725 FT-IR spectrophotometer. Mass spectra were recorded by the “Service de Spectroscopie de Masse” of Paul Sabatier University using FAB (Nermag R10-R10, NBA matrix) or ES (Perkin-Elmer Sciex System API 365). Cyclic voltammograms were obtained with an Autolab system (PGSTAT 100) in dry dimethylformamide (DMF), dichloromethane (DCM), or acetonitrile (0.1 M tetrabutylammonium hexafluorophosphate, TBAH) at 25 °C with a three-electrode system consisting of platinum-disk working (1 mm diameter), platinum-wire counter, and saturated calomel reference electrodes. Electrochemical oxidations were performed by electrolysis with coulometry in dry DMF, dichloromethane or acetonitrile (0.1 M TBAH) at 25 °C at fixed potential with a three-electrode system consisting of platinum-net working, platinum-wire counter, and saturated calomel reference electrodes. EPR experiments were performed in frozen DCM solution (100 K) with a typical concentration of  $5 \times 10^{-4}$  M on a Bruker Elexys 500 E X-band spectrometer (equipped with Bruker NMR teslameter). Magnetization measurements were performed using a conventional SQUID Quantum Design MPMS-5 magnetometer. This magnetometer works between 1.75 and 300 K with a stability of temperature lower than 0.01 K. The magnetic field was obtained using a superconducting magnet (max field  $\pm 5$

(32) Robin, M. B.; Day, P. *Adv. Inorg. Chem. Radiochem.* **1967**, *10*, 247.

(33) Sullivan, B. P.; Calvert, J. M.; Meyer, T. J. *Inorg. Chem.* **1980**, *34*, 1404.

T) which provides a highly uniform field. Measurements were made using the reciprocating sample option (RSO), which provides a high accuracy of dc measurements (SQUID sensitivity of  $10^{-7}$  emu). The sample holder did not give any paramagnetic signal, and its diamagnetic signal was too low compared to the sample signal to give any visible contribution. Diamagnetic susceptibilities corrections for [2][PF<sub>6</sub>] and [3][PF<sub>6</sub>] were taken as  $-639 \times 10^{-6}$  and  $-767 \times 10^{-6}$  cm<sup>3</sup> mol<sup>-1</sup>, respectively, using Pascal's constant.<sup>34</sup>

**5.3. Synthesis of Complexes. Synthesis of [Ru(tpy)(thd)Cl] (1).** [Ru(tpy)Cl<sub>3</sub>] (417 mg, 0.946 mmol) was placed in solution in ethanol (200 mL). The brown suspension was degassed, and the apparatus was flushed with argon and triethylamine (1.4 mL, 11 equiv) and 2,2,6,6-tetramethyl-3,5-heptanedione (1.6 mL, 8 equiv) were added. The mixture was heated under reflux for 2 h. The solution, which had turned dark purple, was allowed to cool at room temperature and then evaporated to dryness. The dark residue was dissolved in dichloromethane (100 mL), and the resulting solution was filtered through Celite, leaving a purple-black solid and a blue-green filtrate, which was evaporated to dryness. Ether was then added to the resulting solid, giving a suspension of a blue-green powder, which was filtered and washed with water and ether before being air-dried (187 mg, 36%). <sup>1</sup>H NMR (CD<sub>2</sub>Cl<sub>2</sub> δ = 5.35): 8.67 (2H, ddd, 5.6, 1.5, and 0.9 Hz); 8.14 (2H, ddd, 8.1, 1.3, and 0.9 Hz); 8.06 (2H, d, 8.0 Hz); 7.79 (2H, ddd, 8.1, 7.5, and 1.5 Hz); 7.48 (2H, ddd, 7.5, 5.6, and 1.3 Hz); 7.43 (1H, t, 8.0 Hz); 5.58 (1H, s); 1.57 (9H, s); 0.45 (9H, s). <sup>13</sup>C NMR (CD<sub>2</sub>Cl<sub>2</sub> δ = 53.48): 195.7, 195.3, 162.0, 159.7, 151.1, 134.6, 126.2, 125.4, 121.0, 119.3, 91.0, 41.6, 40.1, 28.6, 27.5. FAB mass spectrum (DMF) *m/z*: 553 [M]<sup>+</sup> (calcd 553.1); 518 [Ru<sup>II</sup>(tpy)(thd)]<sup>+</sup> (calcd 518.1); 370 [Ru<sup>II</sup>(tpy)Cl]<sup>+</sup> (calcd 370.0). Anal. Calcd for RuC<sub>26</sub>H<sub>30</sub>N<sub>3</sub>O<sub>2</sub>Cl: C, 56.5, H, 5.5, N, 7.6. Found: C, 56.1, H, 5.5, N, 7.5%. CV (DCM, 0.1 M TBAH, 0.1V s<sup>-1</sup>, vs SCE) *E*<sub>1/2</sub>(Ru<sup>II</sup>/Ru<sup>III</sup>) = 0.198 V.

**Synthesis of [Ru(tpy)(thd)(Ipcyd)] (2).** To a dark blue solution of **1** (250 mg, 0.452 mmol) in an ethanol/water mixture (5:1, 120 mL) previously degassed was added silver hexafluorophosphate (238 mg, 0.941 mmol, 2.1 equiv), which caused the solution to turn brown-green. The mixture was heated under reflux for 3.5 h and then allowed to cool before being filtered through Celite. IpcydH (1.15 g, 4.71 mmol, 10.4 equiv) was added to the purple filtrate, and the solution was stirred under argon at 40 °C for 66 h. At this stage, evaporation of the mixture gave a solid, which was purified by column chromatography (weakly acidic alumina; solvent, dichloromethane; eluent, dichloromethane/ethanol 99.2:0.8). The second band (dark blue) was collected, evaporated to dryness, and recrystallized from a mixture of dichloromethane and cyclohexane to give a dark blue powder of **2** (225 mg, 65%). <sup>1</sup>H NMR (CD<sub>2</sub>Cl<sub>2</sub> δ = 5.35): 8.62 (2H, ddd, 5.5, 1.5, and 0.9 Hz); 8.15 (2H, ddd, 8.0, 1.4, and 0.9 Hz); 8.07 (2H, d, 8.0 Hz); 7.86 (2H, ddd, 8.0, 7.6, and 1.5 Hz); 7.52 (1H, t, 8.0 Hz); 7.50 (2H, ddd, 7.6, 5.5, and 1.4 Hz); 7.13 (2H, d, 8.7 Hz); 6.09 (2H, d, 8.7 Hz); 5.64 (1H, s); 1.56 (9H, s); 0.49 (9H, s). <sup>13</sup>C NMR (CD<sub>2</sub>Cl<sub>2</sub> δ = 53.48): 196.9, 196.8, 160.9, 159.6, 153.3, 150.7, 136.9, 135.1, 126.7, 126.0, 125.8, 121.6, 121.3, 120.1, 88.9, 76.5, 41.6, 40.2, 28.7, 27.6. IR *ν*/cm<sup>-1</sup> 2175s (NCN). ES mass spectrum (CH<sub>3</sub>CN) *m/z*: 762.3 [M + H]<sup>+</sup> (calcd 762.1); 546.3 [Ru(tpy)(thd)(HCN) + H]<sup>+</sup> (calcd 546.2). Anal. Calcd for RuC<sub>33</sub>H<sub>34</sub>N<sub>5</sub>O<sub>2</sub>I(H<sub>2</sub>O): C, 50.9; H, 4.7; N, 9.0. Found: C, 50.7; H, 4.6; N, 8.9%. CV (DCM, 0.1 M TBAH, 0.1 V s<sup>-1</sup>, vs SCE) *E*<sub>1/2</sub>(Ru<sup>II</sup>/Ru<sup>III</sup>) = 0.200 V.

**Synthesis of [2][PF<sub>6</sub>].** To a dark blue solution of **2** (100 mg, 0.131 mmol) in dichloromethane (50 mL) previously degassed with

argon was added ferrocenium hexafluorophosphate (55 mg, 0.17 mmol, 1.3 equiv). The solution was stirred under argon at room temperature for 45 min and turned golden brown. The solution was filtered through Celite, and the filtrate was concentrated before cyclohexane was added. The obtained precipitate was filtered and washed successively with cyclohexane and ether before being air-dried to yield a green powder (94 mg, 79%). IR *ν*/cm<sup>-1</sup> 2115s (NCN) and 843s (PF<sub>6</sub>). ES mass spectrum (CH<sub>3</sub>CN) *m/z*: positive mode 761.3 [M]<sup>+</sup> (calcd 761.1); negative mode 145.1 [PF<sub>6</sub>]<sup>-</sup> (calcd 145.0). Anal. Calcd for RuC<sub>33</sub>H<sub>34</sub>N<sub>5</sub>O<sub>2</sub>IPF<sub>6</sub>(C<sub>6</sub>H<sub>12</sub>)<sub>0.2</sub>: C, 44.5; H, 4.0; N, 7.6. Found: C, 44.4; H, 3.9; N, 7.6%.

**Synthesis of [{Ru(tpy)(thd)}<sub>2</sub>(μ-dicyd)][PF<sub>6</sub>] ([3][PF<sub>6</sub>]).** To a dark blue solution of **1** (310 mg, 0.561 mmol) in an ethanol/water mixture (5:1, 120 mL) previously degassed was added silver hexafluorophosphate (283 mg, 1.12 mmol, 2.0 equiv), and the solution turned brown-green. The mixture was heated under reflux for 3 h and then allowed to cool before being filtered through Celite. DicydH<sub>2</sub> (45 mg, 0.28 mmol, 0.51 equiv) was added to the purple filtrate, and the solution was stirred under argon at 40 °C for 48 h. Evaporation of the mixture gave a solid, which was purified by column chromatography (weakly acidic alumina, solvent: dichloromethane, eluent: dichloromethane/ethanol 99:1). The first band (purple) was collected, evaporated to dryness, and recrystallized twice from a mixture of dichloromethane and cyclohexane to give a dark purple powder of **3** (109 mg, 29%). IR *ν*/cm<sup>-1</sup> 2092s (NCN) and 845s (PF<sub>6</sub>). ES mass spectrum (CH<sub>3</sub>CN) *m/z*: 1192.6 [M]<sup>+</sup> (calcd 1192.3); 676.5 [Ru(tpy)(thd)(dicydH) + H]<sup>+</sup> (calcd 676.2); 546.3 [Ru(tpy)(thd)(HCN) + H]<sup>+</sup> (calcd 546.2); 145.1 [PF<sub>6</sub>]<sup>-</sup> (calcd 145.0). Anal. Calcd for Ru<sub>2</sub>C<sub>60</sub>H<sub>64</sub>N<sub>10</sub>O<sub>4</sub>PF<sub>6</sub>: C, 53.9; H, 4.8; N, 10.5. Found: C, 53.7; H, 5.0; N, 10.4%.

**Synthesis of [{Ru(tpy)(thd)}<sub>2</sub>(μ-dicyd)][PF<sub>6</sub>]<sub>2</sub> ([3][PF<sub>6</sub>]<sub>2</sub>).** To a solution of [3][PF<sub>6</sub>] (16.2 mg, 0.012 mmol) in freshly distilled dichloromethane (10 mL) was added ferrocenium hexafluorophosphate (4.8 mg, 0.015 mmol, 1.2 equiv). The solution was stirred under argon at room temperature for 1 h, and its color turned from purple to orange-pink. It was filtered through Celite, and the filtrate was concentrated to 5–10 mL. Cyclohexane (30 mL) was added, and the obtained precipitate was filtered and washed with cyclohexane and ether to yield a dark purple powder of [3][PF<sub>6</sub>]<sub>2</sub> (12.3 mg, 0.008 mmol, 69%). ES mass spectrum (CH<sub>3</sub>CN) *m/z*: positive mode 1337.9 [M<sup>2+</sup>, PF<sub>6</sub><sup>-</sup>]<sup>+</sup> (calcd 1337.3); 596.2 [M]<sup>2+</sup> (calcd 596.2); negative mode 145.3 [PF<sub>6</sub>]<sup>-</sup> (calcd 145.0).

**5.4. Crystal Structure Determination of [3][PF<sub>6</sub>]<sub>2</sub>.** Dark red needles were grown by slow diffusion of cyclohexane into a dichloromethane solution of the complex. The diffraction intensities were collected on a Nonius Kappa CCD diffractometer at a temperature of 298 K, using graphite monochromatic Mo Kα radiation (λ = 0.71073 Å) at a detector distance of 4 cm. The crystallographic cell was found by using EVAL-CCD.<sup>35</sup> The structure was solved using DIRDIFF<sup>36</sup> and refined in the maXus software package.<sup>37</sup> Absorption corrections were performed using SORTAV program "Blessing 1995". The refinement was performed anisotropically for all the non-hydrogen atoms of the complex (SHELXL-97).<sup>38</sup> The hydrogen atoms were localized by difference Fourier synthesis, recalculated, and fixed at 0.97 Å, and then their

(34) Mabbs, F. E.; Machin, D. J. *Magnetism and Transition Metal Complexes*; Chapman and Hall: London, 1973.

(35) Duisenberg, A. J. M. Ph.D. Thesis, Utrecht University, The Netherlands, 1998.

(36) Beurskens, P. T.; Beurskens, G.; de Gelder, R.; Garcia-Granda, S.; Gould, R. O.; Israel, R.; Smits, J. M. M. *The DIRDIF-99 program system*; University of Nijmegen: Nijmegen, The Netherlands, 1999.

(37) Mackay, S.; Gilmore, C. J.; Edwards, C.; Stewart, N.; Shankland, K. *maXus Computer Program for the Solution and Refinement of Crystal Structures*; Nonius, The Netherlands; MacScience, Japan; University of Glasgow, Glasgow: 1999.

**Table 5.** Experimental and Calculated Selected Bond Lengths (Å) and Angles (deg)

	L <sup>2-</sup>	L <sup>-</sup>	L <sup>0</sup>	3 <sup>0</sup>	3 <sup>+</sup>	3 <sup>2+</sup> exp (form A)	3 <sup>2+</sup> exp (form B)	3 <sup>2+</sup> (singlet)
<i>a</i>	1.440	1.453	1.481	1.432	1.449	1.410(13)	1.402(12)	1.461
<i>b</i>	1.425	1.403	1.380	1.418	1.403	1.359(13)	1.348(12)	1.392
<i>c</i>	1.443	1.458	1.484	1.439	1.454	1.396(14)	1.418(11)	1.466
<i>d</i>	1.423	1.382	1.336	1.420	1.385	1.335(12)	1.350(10)	1.361
<i>e</i>	1.323	1.336	1.351	1.290	1.313	1.280(12)	1.287(10)	1.311
<i>f</i>	1.226	1.212	1.201	1.208	1.197	1.152(11)	1.154(10)	1.198
<i>g</i>				2.041	2.053	1.966(6)	1.969(6)	2.001
Ru–N <sub>1</sub>				2.097	2.106	2.099(7)	2.069(6)	2.121
Ru–N <sub>2</sub>				1.964	1.974	1.977(6)	1.946(6)	1.988
Ru–N <sub>3</sub>				2.097	2.106	2.062(6)	2.051(7)	2.121
Ru–O <sub>1</sub>				2.118	2.108	2.053(5)	2.057(5)	2.099
Ru–O <sub>2</sub>				2.095	2.083	2.024(5)	2.039(5)	2.054
α	121.9	122.1	123.0	123.4	123.1	124.4(8)	124.0(7)	125.2
β	173.2	172.7	172.3	174.5	173.8	173.9(10)	173.2(8)	173.1
γ				171.6	171.5	174.0(7)	173.3(6)	170.4

contributions were introduced in the calculations but not refined. There were 4313 reflections [ $I > 2\sigma(I)$ ] used for the 814 parameters, and the *R* value dropped to 0.0665. The full experimental details, atomic parameters, and complete listing of bond lengths and angles are available as Supporting Information.

**5.5. Computational Details.** Calculations were performed with the GAMESS (General Atomic and Molecular Electronic Structure System) software.<sup>39</sup> Complete geometry optimizations were carried out using the density functional theory method with the conventional Becke-3-Lee-Yang-Parr (B3LYP) exchange-correlation functional.<sup>40</sup> Hydrogen atoms were assigned 6-31G basis set. The Stevens-Basch-Krauss-Jasien-Cundari (SBKJC) effective core potential and the corresponding valence basis set<sup>41</sup> were employed for all other atoms including ruthenium. Initial geometries were prepared by a molecular mechanics calculation using the universal force field developed by Rappe and Goddard,<sup>42</sup> in a Cerius environment. The optimized geometries are summarized in the Supporting Information. Representations of the molecular orbitals were obtained using Molekel.<sup>43</sup>

Theoretical study was conducted in order to shed light on the behavior of **3** toward oxidation, in particular with respect to the site of oxidation. The calculation was made using DFT, with a suitable pseudopotential for Ru. In a first step, we investigated the question of geometry.

Dinuclear complex **3** possesses several geometrical degrees of freedom. Concerning the ancillary ligands, the conformation of the terpyridine ligand can be considered locked, and the four *tert*-butyl groups on the thd ligands are in almost free rotation. Concerning the geometry of the bridging ligand, the cyanamide groups are almost linear, but two degrees of freedom can be identified on each moiety (see Figure 12): the dihedral angle  $\theta_1$  (C<sub>1</sub>–N<sub>5</sub>–C<sub>2</sub>–C<sub>3</sub>) between the phenyl plane and the cyanamide and the angle  $\theta_2$  (N<sub>2</sub>–Ru–N<sub>5</sub>–C<sub>4</sub>) corresponding to the rotation of the whole phenylcyanamide group around the Ru–N bond (like a flag).

(38) Sheldrick, G. M. *Program for the Refinement of Crystal Structures*; University of Göttingen: Göttingen, Germany, 1997.

(39) Schmidt, M. W.; Balbridge, K. K.; Boatz, J. A.; Elbert, S. T.; Gordon, M. S.; Jensen, J. H.; Koseki, K.; Matsumata, N.; Nguyen, K. A.; Su, S.; Windus, T. L.; Dupuis, M.; Montgomery, J. A. *J. Comput. Chem.* **1993**, *14*, 1347.

(40) Becke, A. D. *J. Chem. Phys.* **1993**, *98*, 5648; Lee, C.; Yang, W.; Parr, R. G. *Phys. Rev.* **1988**, *B37*, 785.

(41) Cundari, T. R.; Stevens, W. J. *J. Chem. Phys.* **1993**, *98* (7), 5555. Stevens, W. J.; Basch, H.; Krauss, M. *J. Chem. Phys.* **1984**, *81* (12), 6026. Stevens, W. J.; Krauss, M. J.; Basch, H.; Jasien, P. G. *Can. J. Chem.* **1992**, *70* (2), 612.

(42) Rappé, A. K.; Goddard, W. A. *J. Phys. Chem.* **1991**, *95*, 3358.

(43) Flükiger, P.; Lüthi, H. P.; Portmann, S.; Weber, J. *Molekel*, **4.3**; Manno: Switzerland, 2000–2002. Portmann, S.; Lüthi, H. P. *Chimia* **2000**, *54*, 776.

**Table 6.** Variation of Atomic Charges upon Oxidation of the Complex<sup>a</sup>

fragment	Ru <sub>1</sub>	Ru <sub>2</sub>	dicyd	tpy <sub>1</sub>	tpy <sub>2</sub>	thd <sub>1</sub>	thd <sub>2</sub>
Δ <i>Q</i> (0 → 1+) (Mulliken)	0.01	0.01	0.53	0.14	0.14	0.08	0.08
Δ <i>Q</i> (0 → 1+) (Lowdin)	−0.01	−0.01	0.59	0.14	0.14	0.07	0.07
Δ <i>Q</i> (1+ → 2+) (Mulliken)	−0.02	−0.02	0.40	0.19	0.19	0.13	0.13
Δ <i>Q</i> (1+ → 2+) (Lowdin)	0.03	0.03	0.42	0.16	0.16	0.11	0.11
Δ <i>Q</i> (0 → 2+) (Mulliken)	−0.01	−0.01	0.93	0.34	0.34	0.21	0.21
Δ <i>Q</i> (0 → 2+) (Lowdin)	0.02	0.02	1.01	0.30	0.30	0.18	0.18

<sup>a</sup> Calculated from Mulliken and Lowdin population analyses.

**Table 7.** Total and SOMO Spin Densities ( $\rho_{\alpha-\beta}$  and  $\rho_{\text{SOMO}}$ ) for Complex **3**<sup>a</sup>

fragment	Ru <sub>1</sub>	Ru <sub>2</sub>	dicyd	tpy <sub>1</sub>	tpy <sub>2</sub>	thd <sub>1</sub>	thd <sub>2</sub>
$\rho_{\alpha-\beta}$ (Mulliken)	0.05	0.05	0.92	0.00	0.00	0.00	0.00
$\rho_{\alpha-\beta}$ (Lowdin)	0.06	0.06	0.90	0.00	0.00	0.00	0.00
$\rho_{\text{SOMO}}$ (Mulliken)	0.09	0.09	0.74	0.02	0.02	0.02	0.02

<sup>a</sup> Spin densities broken down into fragment contributions from metal and ligands.

Preliminary work on mononuclear complex [Ru(tpy)(thd)(pcyd)] showed that the rotation  $\theta_2$  is virtually free while there is an appreciable barrier for rotation along  $\theta_1$ , with energy minimum for  $\theta_1 = 0^\circ$  or  $180^\circ$  (work to be published). This was consistent with X-ray observations on different complexes of this type, showing that the values for  $\theta_1$  were always around  $0^\circ$ , whereas  $\theta_2$  could adopt different values:  $41^\circ$ ,<sup>21</sup>  $69^\circ$ ,<sup>20</sup>  $77^\circ$ ,<sup>44</sup>  $116^\circ$  (this work). The value of  $\theta_1$  was thus taken equal to  $0^\circ$  (or  $180^\circ$ ), and the value of  $\theta_2$  was arbitrarily chosen equal to  $0^\circ$ .

In addition, the bridging ligand can adopt either a syn or an anti conformation, corresponding to the following combinations ( $\theta_1 = 0^\circ$  and  $\theta'_1 = 180^\circ$ ) and ( $\theta_1 = 0^\circ$  and  $\theta'_1 = 0^\circ$ ), respectively. X-ray structures of complexes containing the dicyanamidobenzene bridging ligand showed that these complexes usually adopt the anti conformation,<sup>7,10</sup> which should be intuitively more stable. We adopted this conformation for our calculations.

For the sake of comparison, we also optimized the geometry of the free bridging ligand in its dianionic (L<sup>2-</sup>), radical anionic (L<sup>-</sup>), and neutral (L<sup>0</sup>) forms (see Table 5 and Scheme 3).

Orbital contours and optimized coordinates for complexes **3**, **3**<sup>+</sup>, and **3**<sup>2+</sup> are provided in the Supporting Information.

The variations of atomic charges upon oxidation of the binuclear complex **3** are given in Table 6. The total and partial spin densities for **3**<sup>+</sup> are given in Table 7. Finally, Figure 13 displays the correlation diagram of molecular orbitals for the series of ligands

(44) Sondaz, E.; Jaud, J.; Launay, J. P.; Bonvoisin, J. *Eur. J. Inorg. Chem.* **2002**, *8*, 1924.

**Table 8.** Calculated Wavelengths Associated with Electron Transitions between Frontier Molecular Orbitals in Comparison with the UV-vis Spectra for  $L^{2-}$ ,  $L^{\bullet-}$ , and  $L^0$  Species

$\lambda$ (nm)	exptl	HOMO-1 $\rightarrow$ LUMO	HOMO $\rightarrow$ LUMO	HOMO $\rightarrow$ LUMO+1
$L^{2-}$	265–272–294	233	325	
$L^{\bullet-}$	265–272–293	( $\alpha$ -spin) 205	293	
	362–573–620–680	( $\beta$ -spin) 390	547	400
$L^0$	265–272	359	412	206

**Table 9.** Calculated Wavelengths Associated with Frontier Molecular Orbital Electron Transitions in Comparison with the UV-vis Spectra for  $3^0$ ,  $3^+$ , and  $3^{2+}$  Species

$\lambda$ (nm)	exptl	HOMO-1 $\rightarrow$ LUMO	HOMO $\rightarrow$ LUMO	HOMO $\rightarrow$ LUMO+1
$3$	588	603	1582	1493
$3^+$	530–1366	( $\alpha$ -spin) 592	473	574
		( $\beta$ -spin) 700	609	517
$3^{2+}$	472–1290	1004	1241	483

and complexes obtained upon the first two oxidations:  $L^{2-} \rightarrow L^{\bullet-} \rightarrow L^0$  and  $3 \rightarrow 3^+ \rightarrow 3^{2+}$ . To test the validity of the molecular orbital method, we have used the orbital energies to predict the transition energies. Although we have used here normal DFT (and not TD-DFT), there is usually a good correlation between experimental transition energies and orbital energy differences.<sup>45</sup>

For the  $L^{2-} \rightarrow L^{\bullet-} \rightarrow L^0$  series, the observed and calculated wavelengths are given in Table 8.

In the energy correlation diagram of Figure 13 are reported the relative energy positions of the frontier orbitals of  $L^{2-}$ ,  $L^{\bullet-}$ , and  $L^0$  species and of complexes  $3^0$ ,  $3^{1+}$ , and  $3^{2+}$ . For the isolated bridging ligand “dicyd”, the occupied and unoccupied frontier molecular orbitals are stabilized upon oxidation. The stabilization energy value is calculated to be equal to 5 eV for  $L^{2-}/L^{\bullet-}$  and equal to 4 eV for  $L^{\bullet-}/L^0$ . Upon oxidation, the HOMO–LUMO energy gap varied for each degree of oxidation as follow:  $\Delta E_{\text{HOMO-LUMO}} = 3.8$  eV for  $L^{2-}$ , 4.23 ( $\alpha$ ) 2.6 ( $\beta$ ) eV for  $L^{\bullet-}$ , and 3 eV for  $L^0$ .

In the open electron shell  $L^{\bullet-}$ , the spin polarization energy value between the highest  $\alpha$ -spin and  $\beta$ -spin occupied molecular orbitals is equal to 3.5 eV. This polarization is attenuated when  $L^{\bullet-}$  is inserted in complex  $3^+$ .

In Table 9 are reported the wavelengths (in nm) associated with the lowest energy electron transitions calculated (from the MO energies) for the three oxidation forms of the isolated bridging ligand in comparison with the experimental UV-vis absorption spectra band locations. The calculated values are globally in agreement with the UV-vis experimental determinations.

For the complexes, a  $\mu$ -dicyd orbital is always found between a set of  $d_{\pi}$ -thd levels and a set of  $d_{\pi}^*$ -tpy levels. This peculiar orbital is the HOMO in neutral complex  $3$ , a single occupied and spin polarized in  $3^+$ , and it is the LUMO in  $3^{2+}$  (see Figure 13).

In Table 9 are summarized the calculated values of the wavelengths associated with the lowest energy electron transitions for  $3$ ,  $3^+$ , and  $3^{2+}$  complexes in comparison with the experimental UV-vis absorption spectra. For  $3^{2+}$  the UV-vis absorption bands at 472 and at 1290 nm can be attributed, respectively, to the allowed HOMO $\rightarrow$ LUMO+1 ( $(d_{\pi}$ -thd) $\rightarrow(d_{\pi}^*$ -tpy)) and HOMO $\rightarrow$ LUMO ( $(d_{\pi}$ -thd) $\rightarrow(\mu$ -dicyd)) transitions. For  $3^+$  many electron transitions ( $(\mu$ -dicyd) $\rightarrow(d_{\pi}^*$ -tpy),  $(d_{\pi}$ -thd) $\rightarrow(\mu$ -dicyd), and  $(d_{\pi}$ -thd) $\rightarrow(d_{\pi}^*$ -tpy)) can contribute to the absorption band located at 530 nm. For  $3$  the experimental absorption band at 588 nm can be assigned to the HOMO-1 $\rightarrow$ LUMO ( $(d_{\pi}$ -thd) $\rightarrow(d_{\pi}^*$ -tpy)) electron transition. The lowest two electron transitions are calculated to be at 1582 nm (HOMO $\rightarrow$ LUMO) and at 1493 (HOMO $\rightarrow$ LUMO+1); the latter are not observed in the experimental UV-vis spectrum. For complex  $3^+$ , three calculated transitions at 527, 473, and 574 nm can be convoluted to be assigned to the experimental band observed at 530 nm. However, the observed band at 1366 nm cannot be assigned from our calculations.

**Acknowledgment.** The authors thank CNRS and MENRS (M.F.) for financial support, Alain Mari (LCC, Toulouse) for EPR measurements, Yannick Coppel (LCC, Toulouse) for NMR experiments, and Stéphane Ami (CEMES, Toulouse), Jean-Louis Heully, and Fabienne Alary (IRSAMC, Toulouse) for technical help and helpful advice on theoretical calculations. Sylvain Bertaina and Bernard Barbara (Laboratoire Louis Néel, Grenoble) are greatly acknowledged for magnetic susceptibility measurements.

**Supporting Information Available:** X-ray crystallographic files in CIF format for the structure determination of  $[3][\text{PF}_6]_2$ , CCDC 263306. These data can be obtained free of charge via [www.ccdc.cam.ac.uk/data\\_request/cif](http://www.ccdc.cam.ac.uk/data_request/cif), by emailing [data\\_request@ccdc.cam.ac.uk](mailto:data_request@ccdc.cam.ac.uk), or by contacting The Cambridge Crystallographic Data Centre, 12, Union Road, Cambridge CB2 1EZ, U.K.; fax +44 1223 336033. Additional figures. This material is available free of charge via the Internet at <http://pubs.acs.org>.

IC061085T

(45) Guirado, G.; Coudret, C.; Hliwa, M.; Launay, J.-P. *J. Phys. Chem. B* **2005**, *109* (37), 17445.

(46) Kato, R.; Kobayashi, H.; Kobayashi, A. *J. Am. Chem. Soc.* **1989**, *111*, 5224.

(47) Aquino, M. A. S.; Crutchley, R. J.; Lee, F. L.; Gabe, E. J.; Bensimon, C. *Acta Crystallogr., Sect. C: Cryst. Struct. Commun.* **1993**, *C49* (8), 1543.